

NO-A179 387

PERIODIC ORBITS ABOUT ROTATING ASTEROIDS IN FREE SPACE

1/1

(U) AIR FORCE INST OF TECH WRIGHT-PATTERSON AFB OH

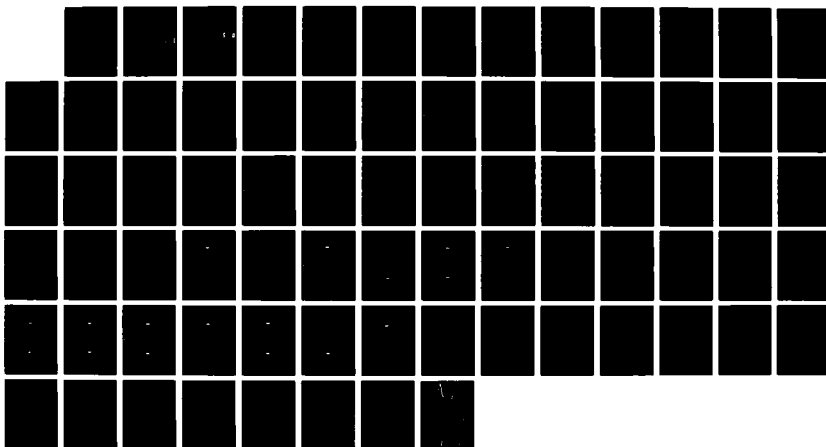
SCHOOL OF ENGINEERING K D HICKS DEC 86

UNCLASSIFIED

AFIT/GA/AA/86D-7

F/B 3/3

NL





XEROCOPY RESOLUTION TEST CHART

DTIC FILE COPY

7

AD-A179 387



PERIODIC ORBITS ABOUT ROTATING
ASTEROIDS IN FREE SPACE
THESIS

Kerry D. Hicks
Second Lieutenant, USAF

AFIT/GA/AA/86D-7

DTIC
ELECTE
APR 16 1987
S
D

DISTRIBUTION STATEMENT A

Approved for public release;
Distribution Unlimited

DEPARTMENT OF THE AIR FORCE
AIR UNIVERSITY

AIR FORCE INSTITUTE OF TECHNOLOGY

Wright-Patterson Air Force Base, Ohio

87 4 16 003

AFIT/GA/AA/86D-7

DTIC
ELECTE
APR 16 1987
S D D

PERIODIC ORBITS ABOUT ROTATING
ASTEROIDS IN FREE SPACE
THESIS

Kerry D. Hicks
Second Lieutenant, USAF

AFIT/GA/AA/86D-7

Approved for public release; distribution unlimited

PERIODIC ORBITS ABOUT ROTATING ASTEROIDS
IN FREE SPACE

THESIS

Presented to the Faculty of the School of Engineering
of the Air Force Institute of Technology
Air University
In Partial Fulfillment of the
Requirements for the Degree of
Master of Science in Astronautical Engineering

Kerry D. Hicks, B.S.
Second Lieutenant, USAF

December 1986



Accession For	
NTIS CRA&I	<input checked="checked" type="checkbox"/>
DTIC TAB	<input type="checkbox"/>
Unannounced	<input type="checkbox"/>
Justification	
By	
Distribution /	
Availability Codes	
Dist	Avail and/or Special
A-1	

Approved for public release; distribution unlimited

Acknowledgments

Upon completion of my thesis, I would like to express my gratitude to my thesis advisor, Dr. William Wiesel. His enthusiasm and assistance helped make this project both educational and enjoyable.

I would also like to express my deepest appreciation to my friend and constant source of encouragement, Laurie. I hope that, in some small way, this finished product justifies her continuous support and belief in me throughout my studies here at AFIT.

Computers used: Osborne I and Heathkit H89
Software used: Wordstar
Printer used: Sanyo PR-5000
Plotter used: HP 7475A

Table of Contents

	Page
Acknowledgements	ii
List of Figures	v
List of Tables	vii
Abstract	viii
I. Introduction	1
II. Problem Dynamics	3
Equations of Motion	3
Potential Energy	4
Kinetic Energy	8
Method of Solution	13
Stability of Orbits	20
Verification and Error Detection	21
Equation Verification	22
Dynamics Verification	22
III. Equilibrium Points	24
Locations in State Space	24
Stability of Equilibrium Points	28
Example Asteroid Calculations	29
Equilibrium Point Results	29
Stability Results	30
IV. Minor Orbits	33

V. Major Orbits	42
Major Orbits With $f > \Omega$	43
5.20 > f > 1.97 Rad/TU	43
1.97 > f > 1.70 Rad/TU	44
1.70 > f > 1.45 Rad/TU	48
1.45 > f > Ω Rad/TU	48
Major Orbits With $f < \Omega$	50
$\Omega > f > 0.60$ Rad/TU	50
0.60 > f Rad/TU	50
Remarks on Major Orbits	51
VI. Conclusion and Recommendations	55
Dynamics and Method of Solution	55
Equilibrium Points	55
Minor Orbits	56
Major Orbits	56
Related Problem for Study	56
Conclusion	56
Appendix A: Fictitious Asteroid Characteristics	57
Appendix B: Variational Matrix	59
Bibliography	62
Vita	63

List of Figures

Figure	Page
1. Asteroid Geometry	2
2. Gravitational Potential	4
3. Polar Coordinates	9
4. Typical Orbits	17
5. Typical Minor Orbit Near Equilibrium Point . .	34
6. Initial Radius -vs- Frequency	34
7. Initial P_{λ} -vs- Frequency	35
8. Typical Minor Orbit Near $f = .44$ Rad/TU . . .	36
9. Initial Radius -vs- Frequency	36
10. Initial P_{λ} -vs- Frequency	37
11. Minor Orbit at $f = .441$ Rad/TU	37
12. Minor Orbit at $f = .321$ Rad/TU	38
13. Minor Orbit at $f = .305$ Rad/TU	38
14. Minor Orbit at $f = .290$ Rad/TU	39
15. Major Orbit at $f = 5.20$ Rad/TU	44
16. Major Orbit at $f = 4.50$ Rad/TU	44
17. Major Orbit at $f = 3.50$ Rad/TU	45
18. Major Orbit at $f = 2.20$ Rad/TU	45
19. Major Orbit at $f = 2.10$ Rad/TU	46
20. Major Orbit at $f = 2.05$ Rad/TU	46
21. Major Orbit at $f = 2.02$ Rad/TU	47
22. Major Orbit at $f = 2.00$ Rad/TU	47
23. Major Orbit at $f = 1.97$ Rad/TU	48

Figure		Page
24.	Major Orbit at $f = 1.70$ Rad/TU	49
25.	Major Orbit at $f = 1.45$ Rad/TU	49
26.	Major Orbit at $f = 0.60$ Rad/TU	50
27.	Major Orbit at $f = 0.50$ Rad/TU	51
28.	Initial Radius -vs- Frequency	53
29.	Initial P_λ -vs- Frequency	54

List of Tables

Table		Page
I.	Typical Asteroid Data	27
II.	Roots of Eq. (4-3a) for Example Asteroid . .	29
III.	Roots of Eq. (4-3b) for Example Asteroid . .	29
IV.	Equilibrium Points for Example Asteroid . .	30
V.	Eigenvalues and Eigenvectors at Stable . . .	31
VI.	Summary of Minor Orbits Computed	40
VII.	Fictitious Asteroid Data (Standard Units) . .	57
VIII.	Fictitious Asteroid Data (Canonical Units) .	58

Abstract

This study investigated periodic orbits about asteroids rotating in free space. Oscillatory orbits about equilibrium points as well as those orbits encircling the body were found. While a method was derived for finding orbits of all inclinations, only equatorial orbits are presented in this report. The major emphasis is on stable, periodic orbits, but certain unstable orbits are presented where appropriate.

The analysis assumed that asteroids could be represented by triaxial ellipsoidal bodies rotating about their major axis of inertia. Hamilton's canonical equations were derived to describe the dynamics. An algorithm was then developed and used to solve the equations of motion in such a way as to find closed, periodic orbits.

PERIODIC ORBITS ABOUT ROTATING ASTEROIDS IN FREE SPACE

I. Introduction

Thousands of asteroids revolve around the Sun, mainly between the orbits of Mars and Jupiter. Some of these are large enough to consider orbiting with a small probe or satellite. There is also evidence that at least a few asteroids have their own natural satellites (1:9-10). For these reasons, this study investigates families of orbits about such bodies.

As is common practice, it is assumed that asteroids have a triaxial ellipsoid shape with axes $a > b > c$ and a rotation about the shortest axis (7:436). (See Figure 1.) Further, the gravitational perturbations of the Sun, planets, and other asteroids are assumed to be negligible (free space). Orbits around such bodies have been investigated in the past, but no previous attempt has been made to find the equations of motion in such a way as to be conducive to numerical solution (3:37-38; 8:707-710; 9:75-84). Also, because these earlier studies did not compute actual orbits, they made no attempt to describe the appearance of such orbits.

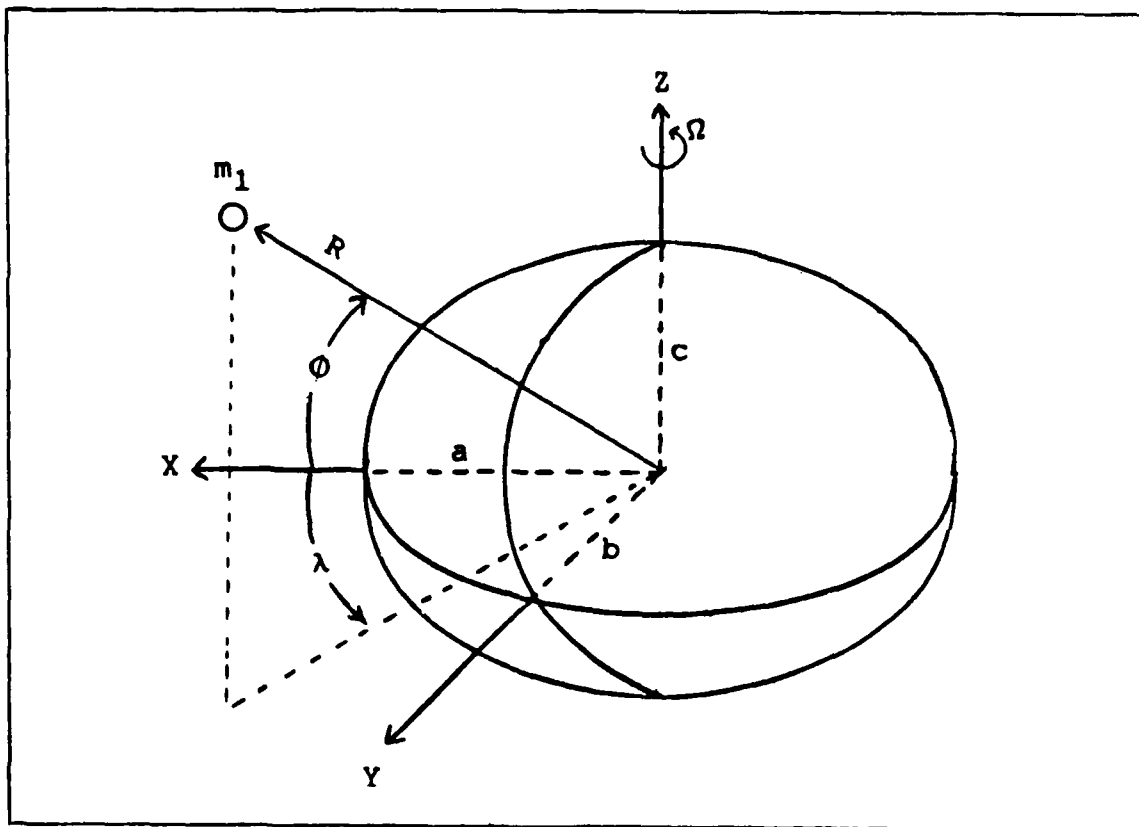


Figure 1: Asteroid Geometry

The specific task in this study is to derive the equations of motion in such a way as to facilitate numerical solution for orbits about an arbitrary triaxial ellipsoid in free space. In process of finding these orbits, the equilibrium points for such bodies will also be investigated. Finally, as an example, the results for a fictitious, but realistic, asteroid will be presented in a graphical format.

II. Problem Dynamics

The problem to be solved is that of finding the motion of a small satellite orbiting an asteroid. It is assumed that the asteroid can be modeled as a triaxial ellipsoid, rotating about its shortest axis with some angular velocity. If the satellite mass is so small as to not effect the motion of the asteroid, then it can be assumed that the center of mass for the system is fixed in inertial space and is located at the center of mass of the asteroid. Further, the problem is restricted to asteroids in free space.

Equations of Motion

The equations of motion are to be numerically solved, so they are derived with this in mind. Most numerical integration packages are written to solve first order differential equations; therefore, the Hamilton canonical equations are derived and used to describe the motion.

The first step in finding the equations of motion is to form the Hamiltonian

$$H = \sum p_i \dot{q}_i - L \quad (2-1)$$

where p_i and \dot{q}_i are the generalized momenta and velocities, respectively. The last term, L , denotes the Lagrangian, defined simply as

$$L = T - V \quad (2-2)$$

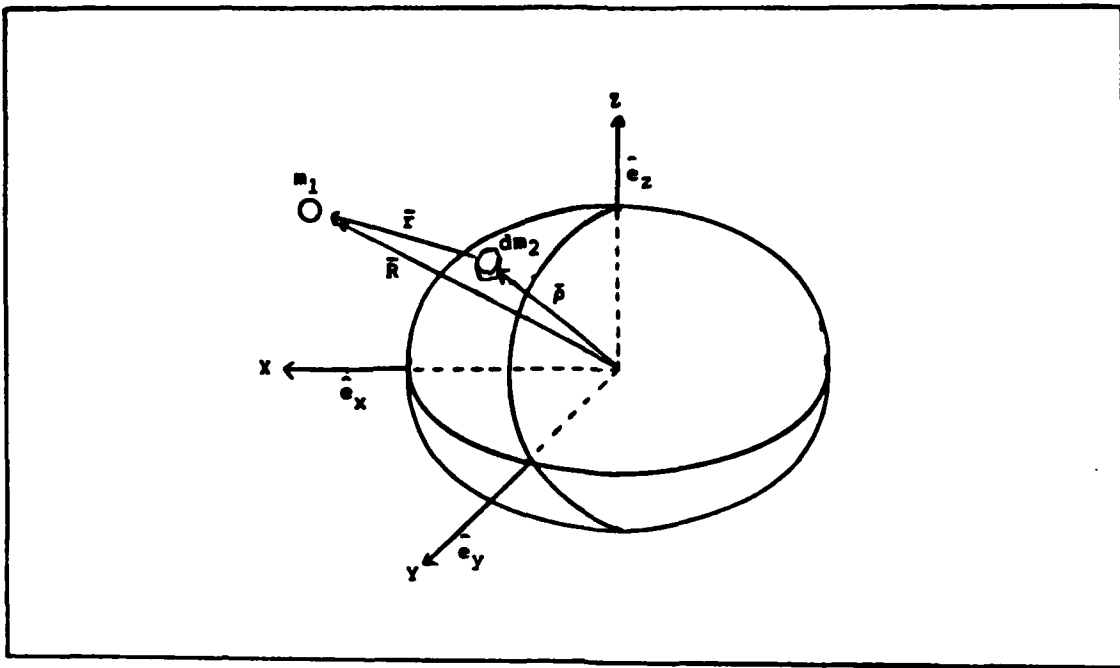


Figure 2: Gravitational Potential

with T and V being the kinetic energy and potential energy of the satellite. It is these two terms that must be determined before the Hamiltonian can be assembled.

Potential Energy. The gravitational attraction of the asteroid on the satellite provides the potential energy and an expression for this can be found (4:431, 434-436). Figure 2 shows the body-fixed (rotating) coordinate system to be used for this calculation. From the figure, it is clear this can be written in the integral form

$$V = -Gm_1 \int (dm_2)/r \quad (2-3)$$

where $r = |\bar{R} - \bar{p}|$ is the distance shown in Figure 2 and G is the Universal Gravitational constant.

The $1/r$ term in Eq. (2-3) can be written:

$$r^{-1} = R^{-1} \left\{ 1 - \left[\frac{2\bar{R} \cdot \bar{\rho}}{R^2} - \left(\frac{\rho}{R} \right)^2 \right] \right\}^{-1/2} \quad (2-4)$$

If it is assumed that the asteroid dimensions are smaller than the distance between the mass centers, then the right-hand side can be expanded in a power series:

$$r^{-1} = R^{-1} \left\{ 1 + \frac{\bar{R} \cdot \bar{\rho}}{R^2} - \frac{1}{2} \left(\frac{\rho}{R} \right)^2 + \frac{3}{8} \left[\frac{2\bar{R} \cdot \bar{\rho}}{R^2} - \left(\frac{\rho}{R} \right)^2 \right]^2 + \dots \right\} \quad (2-5)$$

Carrying out the algebra, this can be rewritten as:

$$r^{-1} = R^{-1} + \frac{\bar{R} \cdot \bar{\rho}}{R^3} - \frac{1}{2} \frac{\rho^2}{R^3} + \frac{3}{2} \frac{(\bar{R} \cdot \bar{\rho})^2}{R^5} + \text{order} \left(\frac{\rho^3}{R^4} \right) \quad (2-6)$$

Using the body-fixed reference frame previously shown in Figure 2 and applying the following definitions

$$\begin{aligned} \bar{\rho} &= x\hat{e}_x + y\hat{e}_y + z\hat{e}_z \\ \bar{R} &= R (l\hat{e}_x + m\hat{e}_y + n\hat{e}_z) \\ \bar{R} \cdot \bar{\rho} &= R (lx + my + nz) \end{aligned} \quad (2-7)$$

where l , m , and n are the appropriate direction cosines, Eq. (2-6) can be substituted into Eq. (2-3) to yield an

expression for the potential. After ignoring the higher order terms and some simplification, this is written as:

$$\begin{aligned}
 V = & \frac{-Gm_1}{R} \int dm_2 - \frac{Gm_1}{R^2} \int (lx + my + nz) dm_2 \\
 & - \frac{Gm_1}{2R^3} \int [3 (lx + my + nz)^2 - (x^2 + y^2 + z^2)] dm_2
 \end{aligned}
 \tag{2-8}$$

The first integral is trivial:

$$\frac{-Gm_1}{R} \int dm_2 = \frac{-Gm_1 m_2}{R}
 \tag{2-9}$$

The second integral becomes zero when the origin of the axis system is placed at the center of mass.

The final term of Eq. (2-8) can be expanded into easily recognizable quantities:

$$\begin{aligned}
 & \frac{Gm_1}{2R^3} \int [3(lx + my + ny)^2 - (x^2 + y^2 + z^2)] dm_2 \\
 & = \frac{Gm_1}{2R^3} \left[(3l^2 - 1) \int x^2 dm_2 + (3m^2 - 1) \int y^2 dm_2 \right. \\
 & \quad + (3n^2 - 1) \int z^2 dm_2 + 6lm \int xy dm_2 \\
 & \quad \left. + 6ln \int xz dm_2 + 6mn \int yz dm_2 \right]
 \end{aligned}
 \tag{2-10}$$

This can be simplified by noting

$$\begin{aligned}\int x^2 dm_2 &= 1/2 \int [(x^2 + z^2) + (x^2 + y^2) - (y^2 + z^2)] dm_2 \\ &= 1/2 (I_{yy} + I_{zz} + I_{xx})\end{aligned}$$

$$\begin{aligned}\int y^2 dm_2 &= 1/2 \int [(x^2 + y^2) + (y^2 + z^2) - (x^2 + z^2)] dm_2 \\ &= 1/2 (I_{zz} + I_{xx} + I_{yy})\end{aligned}$$

$$\begin{aligned}\int z^2 dm_2 &= 1/2 \int [(y^2 + z^2) + (x^2 + z^2) - (x^2 + y^2)] dm_2 \\ &= 1/2 (I_{xx} + I_{yy} + I_{zz})\end{aligned}$$

$$\int xy dm_2 = I_{xy}$$

$$\int xz dm_2 = I_{xz}$$

$$\int yz dm_2 = I_{yz} \quad (2-11)$$

where I_{xx} , I_{yy} , I_{zz} are the mass moments of inertia and I_{xy} , I_{xz} , I_{yz} are the mass products of inertia (4:435-436). If it is assumed that, in addition to originating at the center of mass, the axes are arranged such that I_{xx} , I_{yy} , and I_{zz} are principal moments of inertia, then $I_{xy} = I_{xz} = I_{yz} = 0$.

Clearly, Eq. (2-8) can now be written as:

$$\begin{aligned}
 V = & \frac{-Gm_1m_2}{R} - \frac{Gm_1}{4R^3} [(3l^2 - 1) (I_{yy} + I_{zz} - I_{xx}) \\
 & + (3m^2 - 1) (I_{xx} + I_{zz} - I_{yy}) \\
 & + (3n^2 - 1) (I_{xx} + I_{yy} - I_{zz})] \quad (2-12a)
 \end{aligned}$$

The body-fixed spherical coordinates shown in Figure 3 will prove to be more convenient, so Eq. (2-12a) is rewritten

$$\begin{aligned}
 V = & \frac{-Gm_1m_2}{R} - \frac{Gm_1}{4R^3} [(3\cos^2\phi \cos^2\lambda - 1) (I_{yy} + I_{zz} - I_{xx}) \\
 & + (3\cos^2\phi \sin^2\lambda - 1) (I_{xx} + I_{zz} - I_{yy}) \\
 & + (3\sin^2\phi - 1) (I_{xx} + I_{yy} - I_{zz})] \quad (2-12b)
 \end{aligned}$$

where R is the distance between the mass centers, λ is the longitude measured from the x -axis, and ϕ is the latitude.

Kinetic Energy. The kinetic energy of the satellite is simply

$$T = (1/2)m_1v_{inert}^2 \quad (2-13)$$

where the inertial velocity of the satellite is given by:

$$\bar{v}_{inert} = \bar{v}_{rel} + (\bar{\Omega} \times \bar{R}) \quad (2-14)$$

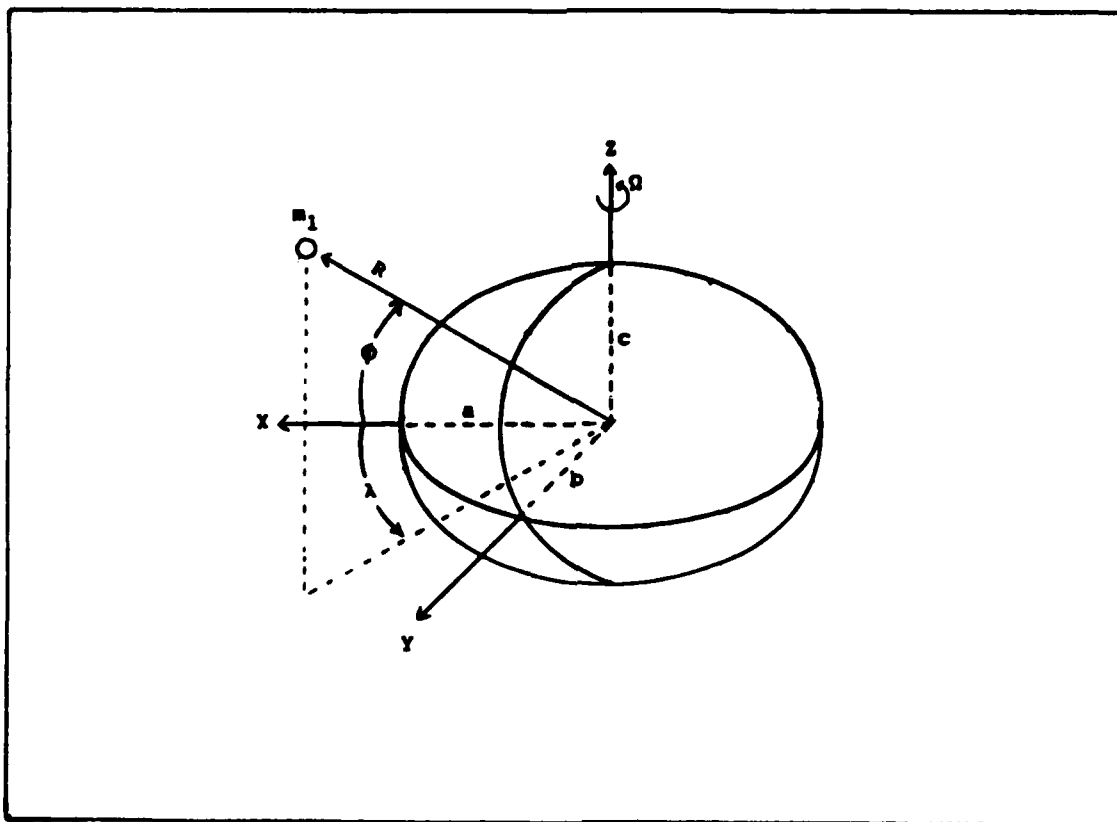


Figure 3: Polar Coordinates

\bar{v}_{rel} is the velocity relative to the asteroid, $\bar{\Omega}$ is the angular velocity of the asteroid, and \bar{R} is the distance between mass centers as was previously defined.

Using the spherical coordinates shown, Eq. (2-14) becomes:

$$\bar{v}_{inert} = R\dot{\phi}\hat{e}_{\phi} + R[(\dot{\lambda} + \Omega)\cos\phi]\hat{e}_{\lambda} + \dot{R}\hat{e}_R \quad (2-15)$$

Thus, the kinetic energy, T , becomes:

$$T = (1/2) m_1 [R^2\dot{\phi}^2 + R^2(\dot{\lambda} + \Omega)^2\cos^2\phi + \dot{R}^2] \quad (2-16)$$

Having found expressions for the potential and kinetic energy, the Lagrangian can now be formed. Substituting Eqs. (2-12b) and (2-16) into Eq. (2-2) results in the following expression for the Lagrangian:

$$\begin{aligned}
 L = & \frac{m_1}{2} [R^2 \dot{\phi}^2 + R^2 (\dot{\lambda} + \Omega)^2 \cos^2 \phi + \dot{R}^2] + \frac{Gm_1 m_2}{R} \\
 & + \frac{Gm_1}{4R^3} [(3\cos^2 \phi \cos^2 \lambda - 1) (I_{yy} + I_{zz} - I_{xx}) \\
 & + (3\cos^2 \phi \sin^2 \lambda - 1) (I_{xx} + I_{zz} - I_{yy}) \\
 & + (3\sin^2 \phi - 1) (I_{xx} + I_{yy} - I_{zz})] \quad (2-17a)
 \end{aligned}$$

Since the mass of the satellite, m_1 , is small and non-zero, it is convenient to divide it out and work with equations on a per unit mass basis. Thus, the Lagrangian is rewritten as:

$$\begin{aligned}
 L = & \frac{1}{2} [R^2 \dot{\phi}^2 + R^2 (\dot{\lambda} + \Omega)^2 \cos^2 \phi + \dot{R}^2] + \frac{Gm_2}{R} \\
 & + \frac{G}{4R^3} [(3\cos^2 \phi \cos^2 \lambda - 1) (I_{yy} + I_{zz} - I_{xx}) \\
 & + (3\cos^2 \phi \sin^2 \lambda - 1) (I_{xx} + I_{zz} - I_{yy}) \\
 & + (3\sin^2 \phi - 1) (I_{xx} + I_{yy} - I_{zz})] \quad (2-17b)
 \end{aligned}$$

The last task before substituting into Eq. (2-1) to find the Hamiltonian is to find expressions for the generalized velocities, \dot{q}_i . This is easily accomplished by using Lagrange's Equations

$$P_\lambda = \frac{\partial L}{\partial \dot{\lambda}} = R^2 (\dot{\lambda} + \Omega) \cos^2 \phi$$

$$P_\phi = \frac{\partial L}{\partial \dot{\phi}} = R^2 \dot{\phi}$$

$$P_R = \frac{\partial L}{\partial \dot{R}} = \dot{R} \quad (2-18)$$

and rearranging to find:

$$\dot{\lambda} = \frac{P_\lambda}{R^2 \cos^2 \phi} - \Omega$$

$$\dot{\phi} = \frac{P_\phi}{R^2}$$

$$\dot{R} = P_R \quad (2-19)$$

The Lagrangian can be rewritten using Eqs. (2-19):

$$\begin{aligned}
 L = & \frac{1}{2} \left[\frac{R^2 p_\phi^2}{R^4} + R^2 \left(\frac{p_\lambda}{R^2 \cos^2 \phi} \right)^2 \cos^2 \phi + p_R^2 \right] + \frac{Gm_2}{R} \\
 & + \frac{G}{4R^3} [(3\cos^2 \phi \cos^2 \lambda - 1) (I_{yy} + I_{zz} - I_{xx}) \\
 & + (3\cos^2 \phi \sin^2 \lambda - 1) (I_{xx} + I_{zz} - I_{yy}) \\
 & + (3\sin^2 \phi - 1) (I_{xx} + I_{yy} - I_{zz})] \quad (2-20)
 \end{aligned}$$

Finally, Eqs. (2-19) and (2-20) can be substituted into Eq. (2-1) to yield the Hamiltonian:

$$\begin{aligned}
 H = & \frac{p_\phi^2}{2R^2} + \frac{p_\lambda^2}{2R^2 \cos^2 \phi} + \frac{p_R^2}{2} - \frac{Gm_2}{R} - \Omega p_\lambda \\
 & - \frac{G}{4R^3} [(3\cos^2 \phi \cos^2 \lambda - 1) (I_{yy} + I_{zz} - I_{xx}) \\
 & + (3\cos^2 \phi \sin^2 \lambda - 1) (I_{xx} + I_{zz} - I_{yy}) \\
 & + (3\sin^2 \phi - 1) (I_{xx} + I_{yy} - I_{zz})] \quad (2-21)
 \end{aligned}$$

Recalling Hamiltonian mechanics and taking the appropriate partial derivatives, Hamilton's canonical equations of motion can be found:

$$\dot{\lambda} = \frac{p_\lambda}{R^2 \cos^2 \phi} - \Omega \quad (2-22a)$$

$$\dot{\phi} = \frac{P_{\phi}}{R^2} \quad (2-22b)$$

$$\dot{R} = P_R \quad (2-22c)$$

$$\dot{P}_{\lambda} = \frac{3G}{R^3} (I_{xx} - I_{yy}) \cos^2 \phi \cos \lambda \sin \lambda \quad (2-22d)$$

$$\begin{aligned} \dot{P}_{\phi} = & \frac{-P_{\lambda}^2 \sin \phi}{R^2 \cos^3 \phi} - \frac{3G}{2R^3} [(\cos^2 \lambda - \sin^2 \lambda) (I_{yy} - I_{xx}) \\ & + (2I_{zz} - I_{xx} - I_{yy})] \cos \phi \sin \phi \end{aligned} \quad (2-22e)$$

$$\begin{aligned} \dot{P}_R = & \frac{-Gm_2}{R^2} - \frac{3G}{4R^4} [(3\cos^2 \phi \cos^2 \lambda - 1) (I_{yy} + I_{zz} - I_{xx}) \\ & + (3\cos^2 \phi \sin^2 \lambda - 1) (I_{xx} + I_{zz} - I_{yy}) \\ & + (3\sin^2 \phi - 1) (I_{xx} + I_{yy} - I_{zz})] \\ & + \frac{P_{\lambda}^2}{R^3 \cos^2 \phi} + \frac{P_{\phi}^2}{R^3} \end{aligned} \quad (2-22f)$$

Method of Solution

The problem to be tackled next is that of integrating the equations of motion to find orbits that are periodic in time. This is done by choosing the initial conditions that

will cause the orbit to return to the same point with the same velocity after the given period. A priori, one does not know these initial conditions, so a method must be derived to find them.

One logical method to go about finding these proper initial conditions is outlined as follows:

- 1) Select an orbital period.
- 2) Guess a set of initial conditions.
- 3) Integrate the equations of motion.
- 4) If the orbit does not return to the same starting point with the same velocity, then vary the initial conditions and repeat step 3.

Step 1 is simply a matter of choice. For Step 2, simple circular orbital motion is assumed to give a fairly good first guess at the initial conditions. The integration in Step 3 is to be performed by Haming, a fourth-order predictor-corrector algorithm (6). Thus, the problem is reduced to finding an efficient means of completing Step 4.

If the coordinates and momenta are assembled into the vector $\bar{x}(t)$, then a general equation of motion can be written:

$$\dot{\bar{x}}(t) = \bar{f}[\bar{x}(t), t] \quad (2-23)$$

Assuming that a reference solution, $\bar{x}_0(t)$, has been found, a nearby orbit can be defined as

$$\bar{x} = \bar{x}_0(t) + \delta\bar{x}(t) \quad (2-24)$$

where $\delta\bar{x}(t)$ is a small displacement in the reference orbit. To a first order approximation, $\delta\bar{x}(t)$ can be shown to be related to a displacement at $t = t_1$ by

$$\bar{x}(t) = \Phi(t, t_1) \delta\bar{x}(t_1) \quad (2-25)$$

Where $\Phi(t, t_1) = \left. \frac{\partial \bar{x}(t)}{\partial \bar{x}(t_1)} \right|_{\bar{x}_0(t)}$ is the state transition

matrix (6:128-129). It can also be shown that the state transition matrix can be found by solving the differential equation

$$\dot{\Phi}(t, t_1) = A(t) \Phi(t, t_1) \quad (2-26)$$

with the boundary condition that $\Phi(t_1, t_1) = I$, the identity matrix (6:130-131). $A(t)$ is the variational matrix and is defined as:

$$A(t) = \left. \frac{\partial \bar{f}}{\partial \bar{x}} \right|_{\bar{x}_0(t)} \quad (2-27)$$

(For reference, the individual terms of the matrix are listed in Appendix B.) Note that, since $A(t)$ is evaluated

along the reference orbit, Eq. (2-26) can be integrated concurrently with the integration of Eq. (2-23).

Now that a reference orbit and the state transition matrix have been found, it remains to use this information to efficiently vary the initial conditions to produce a closed orbit (Step 4). This is a relatively simple procedure and will now be derived.

Figure 4 shows three typical orbits starting at $\lambda = \pi/2$ and continuing for one-half period. If these are truly periodic orbits, then there are certain conditions that must hold due to symmetry. These are clearly

$$\begin{aligned}\lambda(t_2) &= [\lambda(t_1) + n\pi] \\ R^2 \dot{\phi} &= P_{\phi}(t_2) = -P_{\phi}(t_1) \\ \dot{R} &= P_R(t_2) = P_R(t_1) = 0\end{aligned}\tag{2-28}$$

where $\lambda(t_1) = \pi/2$. These can be arranged and placed in a vector:

$$\bar{G} = \begin{bmatrix} \lambda(t_2) - [\lambda(t_1) + n\pi] \\ P_{\phi}(t_2) + P_{\phi}(t_1) \\ P_R(t_2) - P_R(t_1) \end{bmatrix} = \bar{0}\tag{2-29}$$

If this vector, \bar{G} , is evaluated on a reference path, $\bar{x}_0(t)$, that is not a closed orbit, then it will not be equal to zero; instead, it will be equal to some error, \bar{e} . (If it is nearly closed, \bar{e} will be small.)

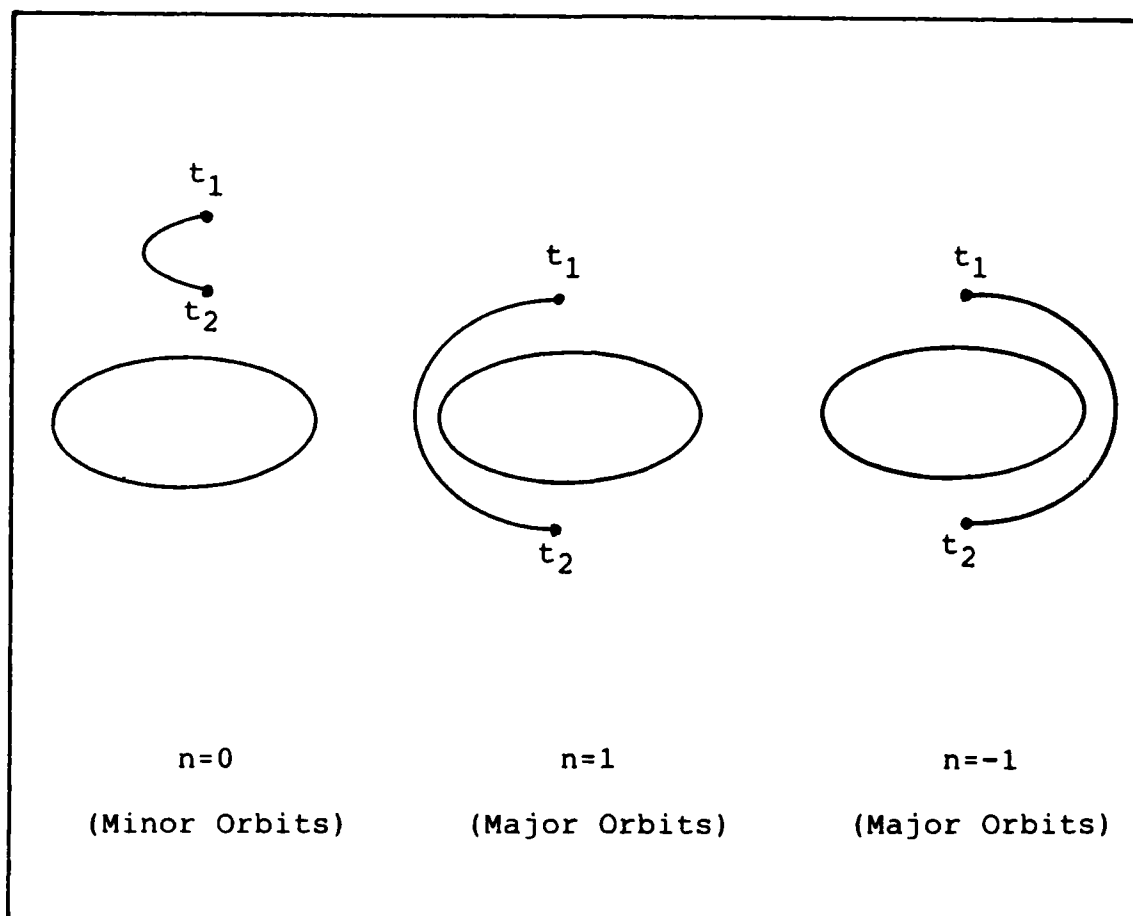


Figure 4: Typical Orbits

For orbits varied slightly from the reference orbit, an expansion of \bar{G} about the reference orbit can be written. To a first order approximation, this is (5:6):

$$\bar{G} [\bar{x}_0(t_2) + \delta \bar{x}(t_2), t_2] \doteq \bar{G} [\bar{x}_0(t_2), t_2] + \left. \frac{\partial \bar{G}}{\partial \bar{x}} \right|_{\bar{x}_0(t_2)} \delta \bar{x}(t_2) \quad (2-30a)$$

More conveniently, this is written as

$$\bar{G} [\bar{x}(t_2), t_2] \doteq \bar{G} [\bar{x}_0(t_2), t_2] + B \delta \bar{x}(t_2) \quad (2-30b)$$

where $B = \left. \frac{\partial \bar{G}}{\partial \bar{x}} \right|_{\bar{x}_0(t_2)}$ and can be easily be shown to be:

$$B = \begin{bmatrix} 1 & 0 & 0 & 0 & 0 & 0 \\ 0 & 0 & 0 & 0 & 1 & 0 \\ 0 & 0 & 0 & 0 & 0 & 1 \end{bmatrix} \quad (2-31)$$

Recall that on the reference path:

$$\bar{G} [\bar{x}_0(t_2), t_2] = \bar{e} \quad (2-32)$$

And, if the varied orbit is a closed orbit, then:

$$\bar{G} [\bar{x}(t_2), t_2] = \bar{0} \quad (2-33)$$

Thus, after substituting Eqs. (2-32) and (2-33) into Eq. (2-30b):

$$B \delta \bar{x}(t_2) = -\bar{e} \quad (2-34)$$

Recall that the problem is to find the variation at $t = t_1$ that makes the varied orbit a closed orbit. Eq. (2-21) relates variations at $t = t_2$ to variations at $t = t_1$. Thus, Eq. (2-34) can be written:

$$B \delta \bar{x}(t_2) = B \Phi(t_2, t_1) \delta \bar{x}(t_1) = -\bar{e} \quad (2-35)$$

The product $B \Phi(t_2, t_1)$ is a 3×6 matrix, so it cannot simply be inverted to find $\delta \bar{x}(t_1)$. However, examining this product in more detail reveals:

$$B \Phi(t_2, t_1) \delta \bar{x}(t_1) = B \Phi(t_2, t_1) \begin{bmatrix} \delta \lambda(t_1) \\ \delta \phi(t_1) \\ \delta R(t_1) \\ \delta P_\lambda(t_1) \\ \delta P_\phi(t_1) \\ \delta P_R(t_1) \end{bmatrix} \quad (2-36)$$

Recalling Eqs. (2-28), the initial conditions $\lambda(t_1)$, $P_\phi(t_1)$, and $P_R(t_1)$ were set and not allowed to vary; therefore, their corresponding variations at $t = t_1$ are zero. This allows the first, fifth, and sixth columns of the product to be eliminated from consideration:

$$[B \Phi(t_2, t_1) \delta \bar{x}(t_1)]_{234} = [B \Phi(t_2, t_1)]_{234} \begin{bmatrix} \delta \lambda(t_1) \\ \delta \phi(t_1) \\ \delta P_\lambda(t_1) \end{bmatrix} \quad (2-37)$$

Using this reduced form, Eq. (2-35) can now be written:

$$[B \Phi(t_2, t_1)]_{234} \begin{bmatrix} \delta \lambda(t_1) \\ \delta \phi(t_1) \\ \delta P_\lambda(t_1) \end{bmatrix} = -\bar{e}_{234} = -\{\bar{G}[\bar{x}(t_2), t_2]\}_{234} \quad (2-38)$$

The reduced product is a square matrix and can be inverted to solve for $\delta \bar{x}(t_1)$:

$$\begin{bmatrix} \delta \lambda(t_1) \\ \delta \phi(t_1) \\ \delta P_\lambda(t_1) \end{bmatrix} = -[B \Phi(t_2, t_1)]_{234}^{-1} \{\bar{G}[\bar{x}(t_2), t_2]\}_{234} \quad (2-39)$$

Using this solution in Eq. (2-24), the initial conditions can be corrected. Note that, since first order approximations have been made at various steps, this correction may not result in a closed orbit. However, if the initial reference orbit is close enough, then the correction will produce a solution that is closer to a closed orbit. Thus, simple iteration is all that is needed to complete Step 4.

For reference in later chapters, it is important to note that the \bar{G} vector is all that determines the type of orbit that will be found. The value of n will determine if it is a minor or a major orbit. (Figure 4 shows the result of this selection.) The choice of $P_\phi(t_1)$ determines the inclination of the orbit. [Selecting $P_\phi(t_1) = 0$ results in equatorial orbits.]

Stability of Orbits

Once a periodic orbit has been found, it is useful to know if it is stable. Since this is a Floquet problem, the condition necessary to determine stability is well

documented (4:264-270; 6:143-148). For this reason the criterion for stability will be stated and used here without proof.

The stability of the orbit is governed by the character of the Poincare' exponents, λ_i , as defined by the determinant

$$| \Phi[(t_1 + \tau), t_1] - \exp(\lambda_i \tau) I | = 0 \quad (2-40)$$

where τ is the period of the orbit (6:144). Note that the terms $\alpha_i = \exp(\lambda_i \tau)$ are simply the eigenvalues of $\Phi[(t_1 + \tau), t_1]$ and that the Poincare' exponents are given by:

$$\lambda_i = (1/\tau) \log_e(\alpha_i) \quad (2-41)$$

If the orbit is stable, then the λ_i 's must all be purely imaginary (4:268; 6:142).

Notice that, after integrating Eqs. (2-23) and (2-26) for an entire orbit, $\Phi[(t_1 + \tau), t_1]$ has been found. Thus, it is a relatively minor addition to calculate the Poincare' exponents and, therefore, determine the stability of the orbit.

Verification and Error Detection

Long derivations and the use of a computer invite the introduction of errors. With this in mind, two tests were used help verify that the results were accurate.

Equation Verification. A simple method can be derived to simultaneously verify that both the equations of motion, \bar{f} , and the variation matrix, $A(t)$, have been entered into the computer correctly. This is done by recalling the definition:

$$A(t) = \left. \frac{\partial \bar{f}}{\partial \bar{x}} \right|_{\bar{x}_0(t)} \quad (2-42)$$

Each term of $A(t)$ can be approximated by

$$a_{ij} = \frac{\partial f_i}{\partial x_j} \doteq \frac{f_i[(x_j + \Delta x_j), t] - f_i[(x_j - \Delta x_j), t]}{2 \Delta x_j} \quad (2-43)$$

where Δx_j is a sufficiently small number.

Thus, for any point, the terms a_{ij} can be calculated exactly using the equations in Appendix B and approximately by using Eq. (2-39). If the values do not approach the same limit as Δx_j gets small, then an error exists in either the equations of motion or in the variation matrix. (It was found that a typical error resulted in differences of at least 25%.) This method of numerical differentiation was used in verifying the program used to generate the results in this paper.

Dynamics Verification If, during the numerical integration, the orbit passes too close to a singularity in the equations of motion, it is possible that the path will cease to be realistic. "Too close" is an ambiguous limitation on

the problem, so it would be useful if some way could be found to detect when it occurs. Fortunately, there is a simple method to detect when this (or any other unforeseen anomaly) causes the integration of the problem dynamics to break down.

Since the Hamiltonian is not a function of time for this problem, it is a constant for all points on any given orbit. Thus, if the Hamiltonian changes suddenly from one point to the next along the path, it is very probable that the limitations on the dynamics have been exceeded. This simple check was performed automatically at each integration point.

III. Equilibrium Points

The equilibrium points will prove to be important starting points in the computation of orbits. Thus, it is advantageous to solve for them first. The procedure for doing this is simple and yields a closed-form solution.

Locations in State Space

Equilibrium points, by definition, are points in state space from which the satellite will not move if it is placed exactly there. In equation form, this condition can be written:

$$\dot{\bar{x}} = \bar{0} \quad (3-1)$$

Referring to Eqs. (2-22), it is clear that a system of six equations in six unknowns is produced:

$$\frac{P_{\lambda}}{R^2 \cos^2 \phi} - \Omega = 0 \quad (3-2a)$$

$$\frac{P_{\phi}}{R^2} = 0 \quad (3-2b)$$

$$P_R = 0 \quad (3-2c)$$

$$\frac{3G}{R^3} (I_{xx} - I_{yy}) \cos^2 \phi \cos \lambda \sin \lambda = 0 \quad (3-2d)$$

$$\frac{-P_{\lambda}^2 \sin \phi}{R^2 \cos^3 \phi} - \frac{3G}{2R^3} [(\cos^2 \lambda - \sin^2 \lambda) (I_{yy} - I_{xx}) + (2I_{zz} - I_{xx} - I_{yy})] \cos \phi \sin \phi = 0 \quad (3-2e)$$

$$\begin{aligned} \frac{-Gm_2}{R^2} - \frac{3G}{4R^4} [(3\cos^2 \phi \cos^2 \lambda - 1) (I_{yy} + I_{zz} - I_{xx}) \\ + (3\cos^2 \phi \sin^2 \lambda - 1) (I_{xx} + I_{zz} - I_{yy}) \\ + (3\sin^2 \phi - 1) (I_{xx} + I_{yy} - I_{zz})] \\ + \frac{P_{\lambda}^2}{R^3 \cos^2 \phi} + \frac{P_{\phi}^2}{R^3} = 0 \end{aligned} \quad (3-2f)$$

After some simple manipulation, the system can be reduced to give the following set of points:

$$(\lambda, \phi, R, P_{\lambda}, P_{\phi}, P_R) = (0, 0, R_1, R_1^2, 0, 0) \quad (3-3a)$$

$$(\lambda, \phi, R, P_{\lambda}, P_{\phi}, P_R) = \left(\frac{\pi}{2}, 0, R_2, R_2^2, 0, 0 \right) \quad (3-3b)$$

$$(\lambda, \phi, R, P_{\lambda}, P_{\phi}, P_R) = (\pi, 0, R_1, R_1^2, 0, 0) \quad (3-3c)$$

$$(\lambda, \phi, R, P_{\lambda}, P_{\phi}, P_R) = \left(\frac{3\pi}{2}, 0, R_2, R_2^2, 0, 0 \right) \quad (3-3d)$$

The terms R_1 and R_2 represent all of the physically realistic roots of the two equations that result from

substituting the values for λ , ϕ , P_ϕ , and P_R along with the expression for P_λ into Eq. (3-2f). These equations are:

$$R_1^5 - Gm_2 R_1^2 - \frac{3G}{2} (I_{zz} + I_{yy} - 2I_{xx}) = 0 \quad (3-4a)$$

$$R_2^5 - Gm_2 R_1^2 - \frac{3G}{2} (I_{zz} + I_{xx} - 2I_{yy}) = 0 \quad (3-4b)$$

Note that the number of equilibrium points depends on the number of physically realistic roots of Eqs. (3-4). Unfortunately, it is impossible, by simple inspection, to determine a general rule regarding the number of the realistic roots. For this reason, seven actual asteroid-like bodies were examined. The results were then analyzed to see what, if any, conclusions could be drawn about the typical nature of the roots and, therefore, the radii of the equilibrium points. [For reference, the approximate dimensions, mass, and rotation rate used for each of these bodies are given in Table I (1:10; 2:138; 7:452).]

These calculations did, indeed, reveal information about the general nature of the roots. Since every body examined exhibited the same trends, it can be concluded that the results from these calculations are typical of realistic asteroids. Thus, the following generalities can be made:

1. Eq. (3-4a) has only one real root. This root, R_1 , has a magnitude that represents a radius slightly greater than that required for a synchronous orbit about an equivalent spherical body.
2. Eq. (3-4b) has three real roots. Two of these roots represent radii so small as to be inside the body; therefore, there is only one realistic root, R_2 , for this equation also. R_2 has a magnitude slightly less than that required for a synchronous orbit about an equivalent spherical body.
3. Because Eqs. (3-4) have only one realistic root each, there are exactly four equilibrium points given by Eqs. (3-3).

Table I: Typical Asteroid Data

Name	Axes Lengths			Ω (rad/s)	Mass (kg)
	a (km)	b (km)	c (km)		
Hebe	114.0	92.0	92.0	2.39×10^{-4}	1.15×10^{19}
Hektor	170.0	63.9	56.5	2.53×10^{-4}	7.33×10^{18}
Juno	137.0	112.0	112.0	2.42×10^{-4}	2.05×10^{19}
Nysa	40.9	27.1	23.0	2.73×10^{-4}	3.04×10^{17}
Pallas	311.0	272.0	272.0	2.21×10^{-4}	2.75×10^{20}
Psyche	142.0	107.0	84.9	4.06×10^{-4}	1.54×10^{19}
Phobos	13.3	11.0	9.2	2.28×10^{-4}	1.61×10^{16}

Stability of Equilibrium Points

An equilibrium point is stable if the eigenvalues of the variation matrix, A , are all purely imaginary (4:222; 6:138-140). The eigenvalues calculated using:

$$| A - \lambda_i I | = 0 \quad (3-5)$$

where A is evaluated at the equilibrium point in question and the λ_i 's are the eigenvalues at that point.

It would be extremely difficult to find a general solution for the eigenvalues in Eq. (3-5). Fortunately, it is not necessary to find a general solution to determine the stability of the points. This is because the equilibrium points for the bodies in Table I were substituted into Eq. (3-5) and, once again, all seven examples yielded the same results. These results, with reasonable certainty, can be considered to be general for typical asteroids and are stated as follows:

1. The points at $\lambda = 0$ and $\lambda = \pi$ are unstable equilibrium points. These points are described completely by Eq. (3-3a) and Eq. (3-3c).
2. The points at $\lambda = \pi/2$ and $\lambda = (3\pi)/2$ are stable equilibrium points. These points are described completely by Eq. (3-3b) and Eq. (3-3d).

Example Asteroid Calculations

As an example, the equilibrium points for the fictitious asteroid of Appendix A were calculated and checked for stability. The results of these calculations are summarized in the following sections.

Equilibrium Point Results. The first step in calculating these points was to find the roots of Eqs. (3-4). These roots, as well as R_1 and R_2 , are listed in Table II and Table III, respectively. (Note that the roots follow

Table II: Roots of Eq. (4-3a) for Example Asteroid

$$\begin{aligned} & (-5.113402188516e-01) + (8.484056878152e-01)i \\ & (-5.113402188516e-01) + (-8.484056878152e-01)i \\ & (1.850707134977e-03) + (2.466559517092e-01)i \\ & (1.850707134977e-03) + (-2.466559517092e-01)i \\ & (1.018979023433e+00) + (0.000000000000e+00)i \end{aligned}$$

$$R_1 = 1.018979023433 \text{ LU}$$

Table III: Roots of Eq. (4-3b) for Example Asteroid

$$\begin{aligned} & (-4.953656785376e-01) + (8.741840563661e-01)i \\ & (-4.953656785376e-01) + (-8.741840563661e-01)i \\ & (-1.694701567977e-01) + (0.000000000000e+00)i \\ & (1.703036684758e-01) + (0.000000000000e+00)i \\ & (9.898978453971e-01) + (0.000000000000e+00)i \end{aligned}$$

$$R_2 = 0.9898978453971 \text{ LU}$$

the generalities stated on page 27.) Using these values for R_1 and R_2 , the equilibrium points were found with Eqs. (3-3) and are shown in Table IV.

Stability Results. The final conclusions of the stability calculations are given in Table IV. While the determination of stability was the main goal of solving the eigenvalue problem, it is interesting to note the information that can be obtained from the actual solutions for the stable equilibrium points.

The magnitudes of the eigenvalues give frequencies at which to start searching for oscillatory orbits near these points, while the eigenvectors give information about the

Table IV: Equilibrium Points for Example Asteroid

Point	λ	ϕ	R	P_λ	P_ϕ	P_R	Stability
1	0	0	R_1	$P_{\lambda 1}$	0	0	Unstable
2	$\frac{\pi}{2}$	0	R_2	$P_{\lambda 2}$	0	0	Stable
3		0	R_1	$P_{\lambda 1}$	0	0	Unstable
4	$\frac{3\pi}{2}$	0	R_2	$P_{\lambda 2}$	0	0	Stable
$R_1 = 1.018979023433 \text{ LU}$				$P_{\lambda 1} = 1.0386121930138 \text{ LU}_2/\text{TU}$			
$R_2 = 0.989897843297 \text{ LU}$				$P_{\lambda 2} = 0.9801751485797 \text{ LU}_2/\text{TU}$			

initial perturbation in direction and momenta from these points (6:140-141). [In later computations of oscillatory (minor) orbits, it was found that the eigenvalues and eigenvectors were of little use other than the determination of stability.] The eigenvalues and eigenvectors are listed in Table V for reference.

Table V: Eigenvalues and Eigenvectors at Stable
Equilibrium Points

	$\lambda_{1,2} = (\pm 0.4960063637745e+00)i$
$\bar{E}_{1,2} =$	$\begin{bmatrix} (-0.9391331508767e+00) + (0.000000000000e+00)i \\ (0.000000000000e+00) + (0.000000000000e+00)i \\ (0.000000000000e+00) + (\pm 0.2894518434642e+00)i \\ (0.000000000000e+00) + (\pm 0.1167656750469e+00)i \\ (0.000000000000e+00) + (0.000000000000e+00)i \\ (-0.1435699563645e+00) + (0.000000000000e+00)i \end{bmatrix}$
	$\lambda_{3,4} = (\pm 0.8673722342857e+00)i$
$\bar{E}_{3,4} =$	$\begin{bmatrix} (-0.8799966095281e+00) + (0.000000000000e+00)i \\ (0.000000000000e+00) + (0.000000000000e+00)i \\ (0.000000000000e+00) + (\pm 0.3953216071260e+00)i \\ (0.000000000000e+00) + (\pm 0.6043478055486e-01)i \\ (0.000000000000e+00) + (0.000000000000e+00)i \\ (-0.3428909856343e+00) + (0.000000000000e+00)i \end{bmatrix}$

(Table continued on next page.)

Table V (Continued):

$$\begin{aligned} & \lambda_{5,6} = (\pm 1.001386855817e+00)i \\ \bar{E}_{5,6} = & \left[\begin{array}{l} (0.000000000000e+00) + (0.000000000000e+00)i \\ (-0.7137642827302e+00) + (0.000000000000e+00)i \\ (0.000000000000e+00) + (0.000000000000e+00)i \\ (0.000000000000e+00) + (0.000000000000e+00)i \\ (0.000000000000e+00) + (\pm 0.7003859997878e+00)i \\ (0.000000000000e+00) + (0.000000000000e+00)i \end{array} \right] \end{aligned}$$

IV. Minor Orbits

Minor orbits are those orbits that are merely oscillations about the stable equilibrium points. This chapter will present minor orbits that lie in the equatorial plane for the example asteroid described in Appendix A. Note that, since the orbits about the two equilibrium points are simply mirror images of each other, it is only necessary to solve for the orbits about one point. For convenience, the point at $\lambda = \pi/2$ was used.

As shown in Chapter II, the \bar{G} vector determines the characteristics of the orbit that will be found by the numerical method. If the integration is to be started at $\lambda = \pi/2$, the \bar{G} vector is:

$$\bar{G} = \begin{bmatrix} \lambda(t_2) - (\pi/2) \\ P_\phi(t_2) \\ P_R(t_2) \end{bmatrix} \quad (4-1)$$

Using this \bar{G} vector, minor orbits can be found using the equations and methods derived in Chapter II.

Orbits were found very near these equilibrium points. A typical example of this family of orbits is shown in Figure 5. The initial conditions are plotted against the frequencies of these orbits in Figures 6 and 7. Note that below a frequency of approximately .47 rad/TU, the orbits became unstable.

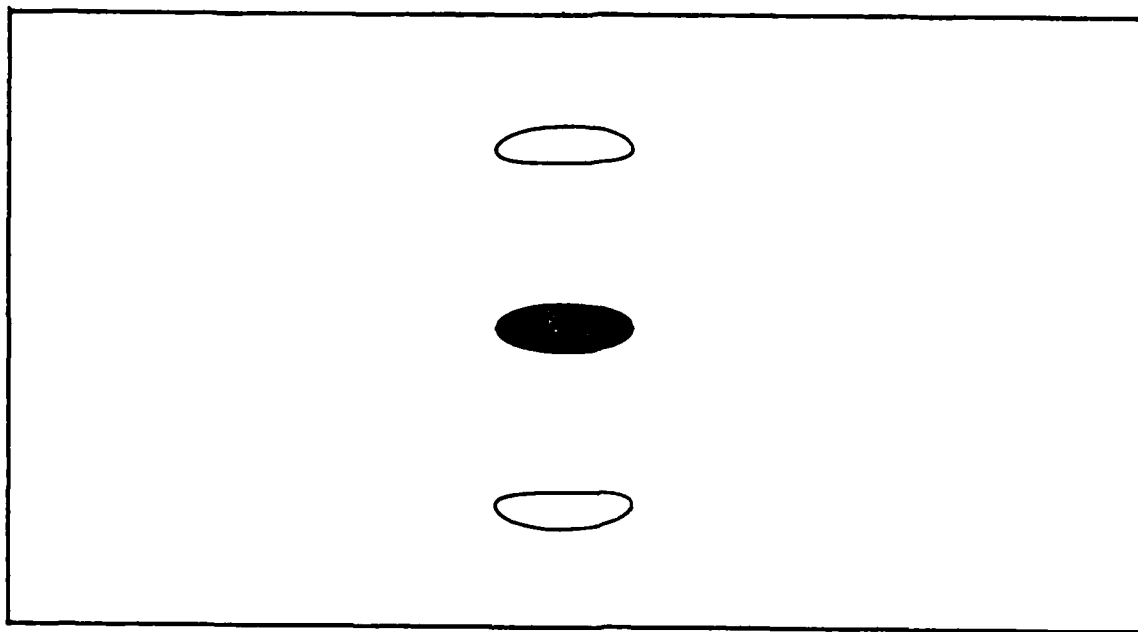


Figure 5: Typical Minor Orbit Near Equilibrium Point

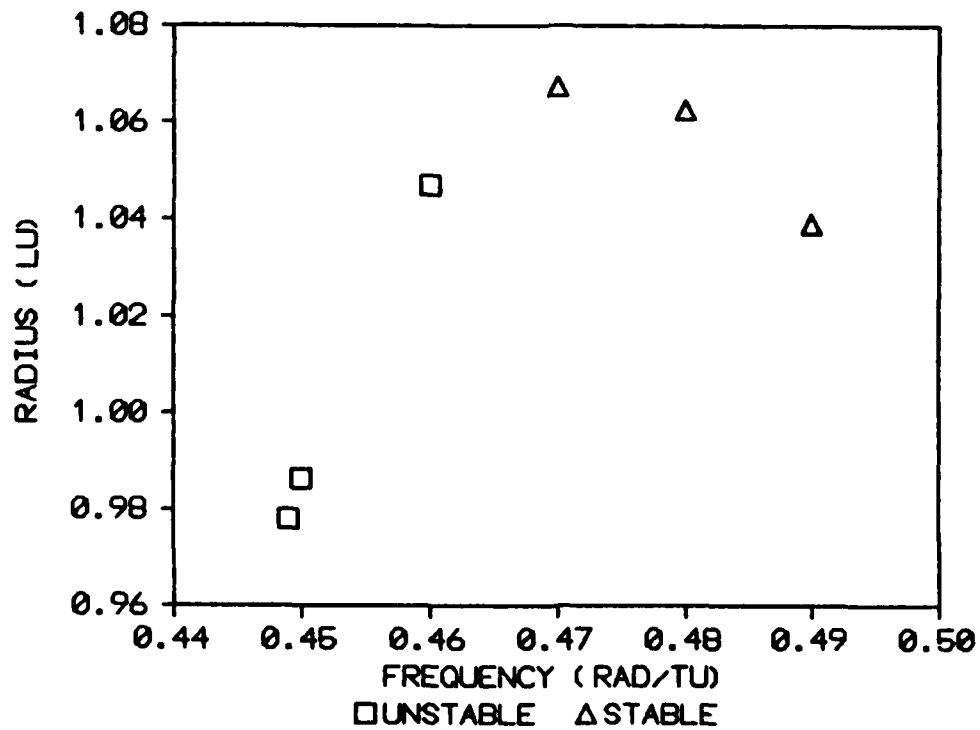


Figure 6: Initial Radius -vs- Frequency

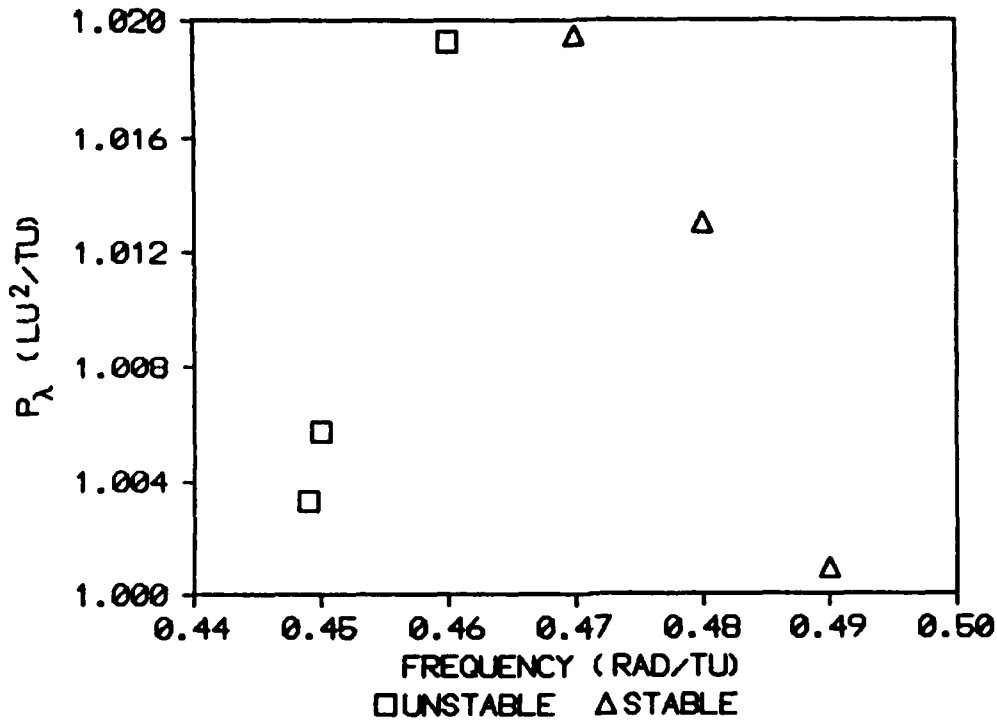


Figure 7: Initial P_λ -vs- Frequency

Another family of stable orbits was found starting at a frequency of approximately .44 rad/TU. A typical example of this family is shown in Figure 8. Radii and momenta data are given in Figures 9 and 10, respectively. Note that the orbits of this family become unstable near a frequency of .395 rad/TU.

No other families of stable orbits were found. There were, however, other interesting orbits computed. Examples of a few of these are shown in Figures 11 - 14 along with the initial conditions of R and P_λ used to compute them. (In all cases, this radius is the maximum radius at which the orbit crosses perpendicular to the y-axis.) Table VI summarizes all of the minor orbits found.

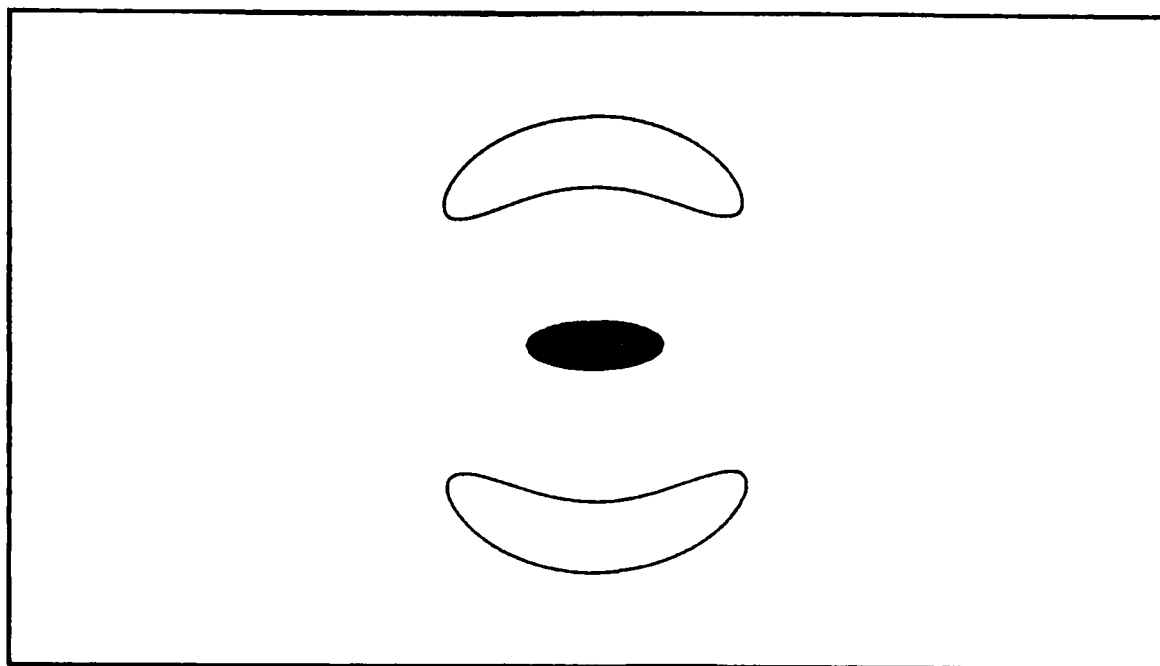


Figure 8: Typical Minor Orbit Near $f = .44$ Rad/TU

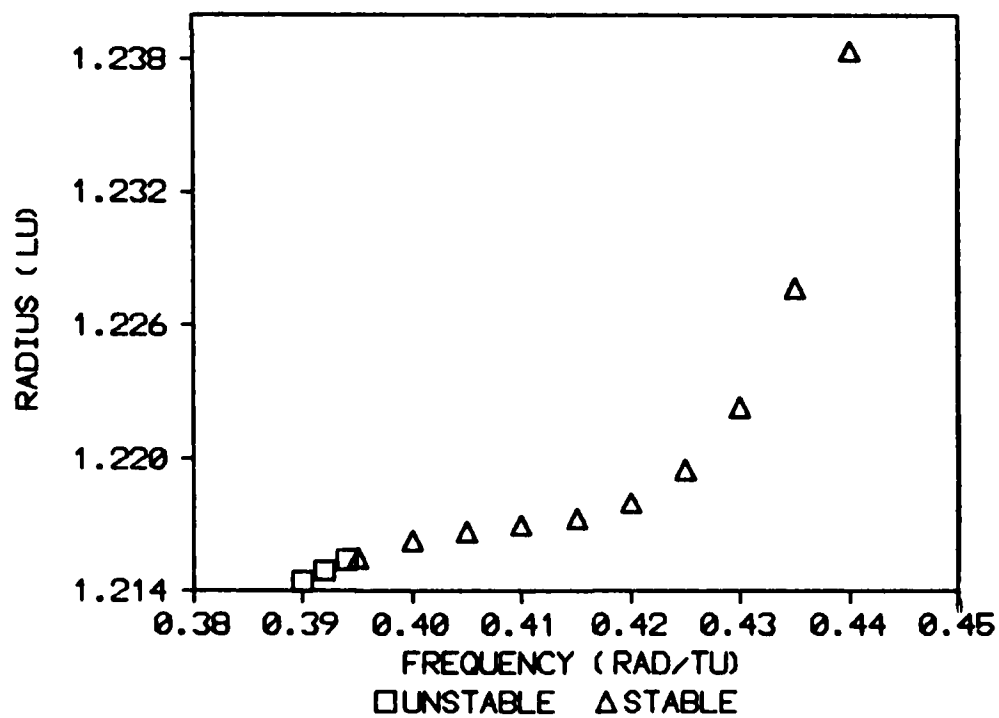


Figure 9: Initial Radius -vs- Frequency

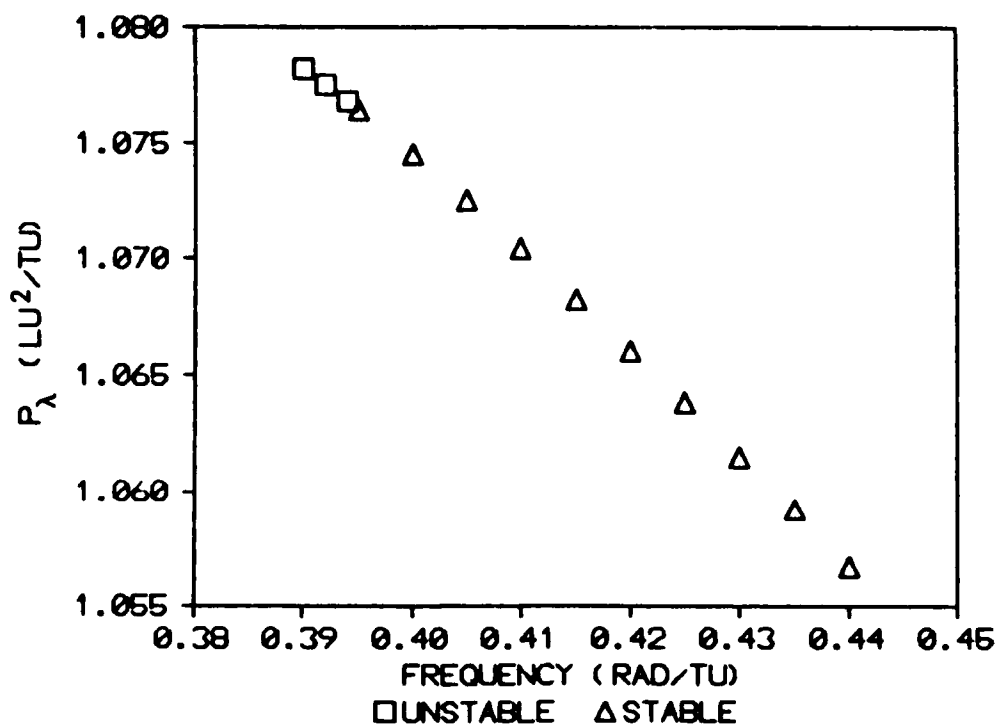


Figure 10: Initial P_λ -vs- Frequency

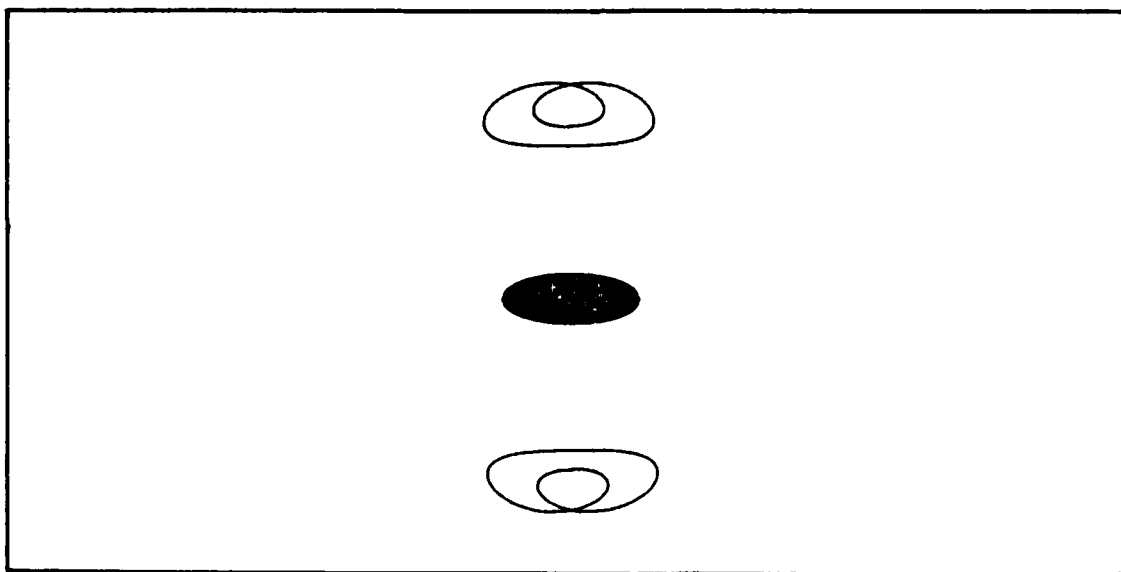


Figure 11: $f = .441$ Rad/TU, $R = 0.9004120106766$ LU,
 $P_\lambda = 0.7992199550355$ LU²/TU

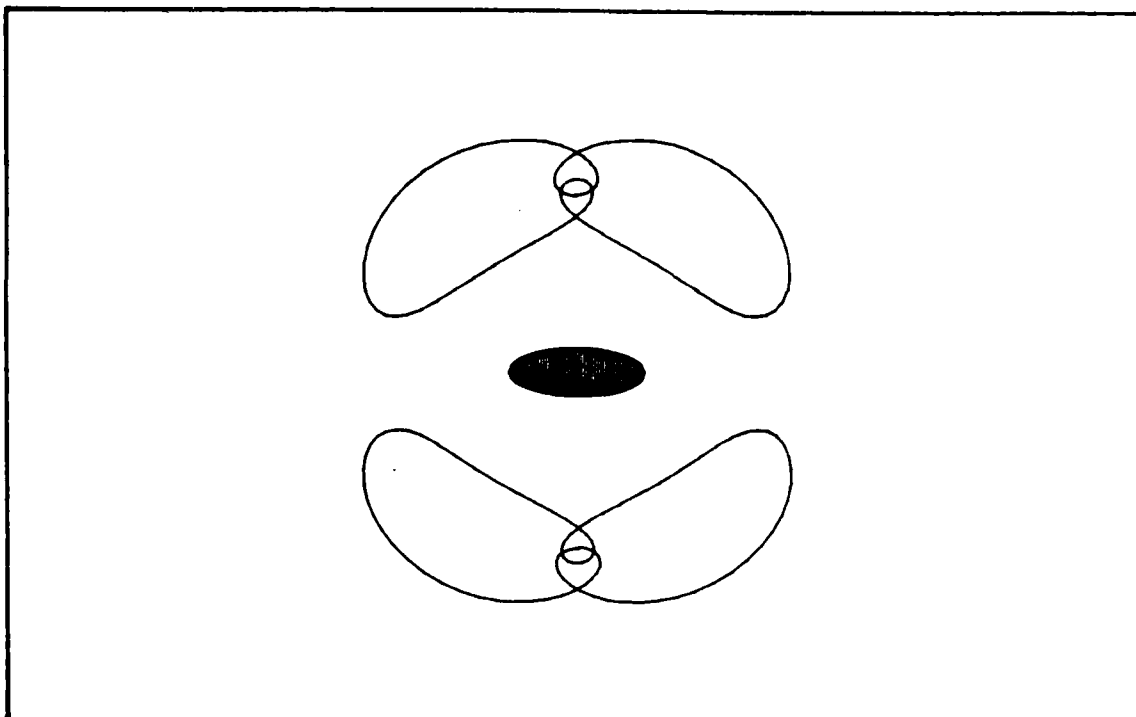


Figure 12: $f = .321 \text{ Rad/TU}$, $R = 1.019464633106 \text{ LU}$,
 $P_{\lambda} = 0.8960785897863 \text{ LU}^2/\text{TU}$

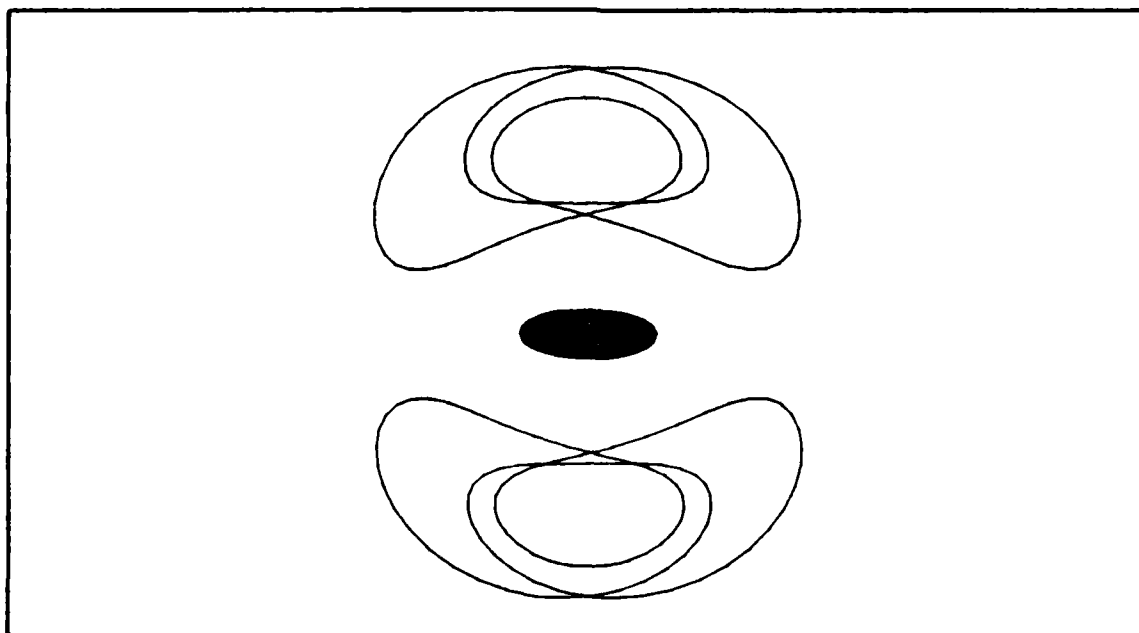


Figure 13: $f = .305 \text{ Rad/TU}$, $R = 1.239528500246 \text{ LU}$,
 $P_{\lambda} = 0.9255337942752 \text{ LU}^2/\text{TU}$

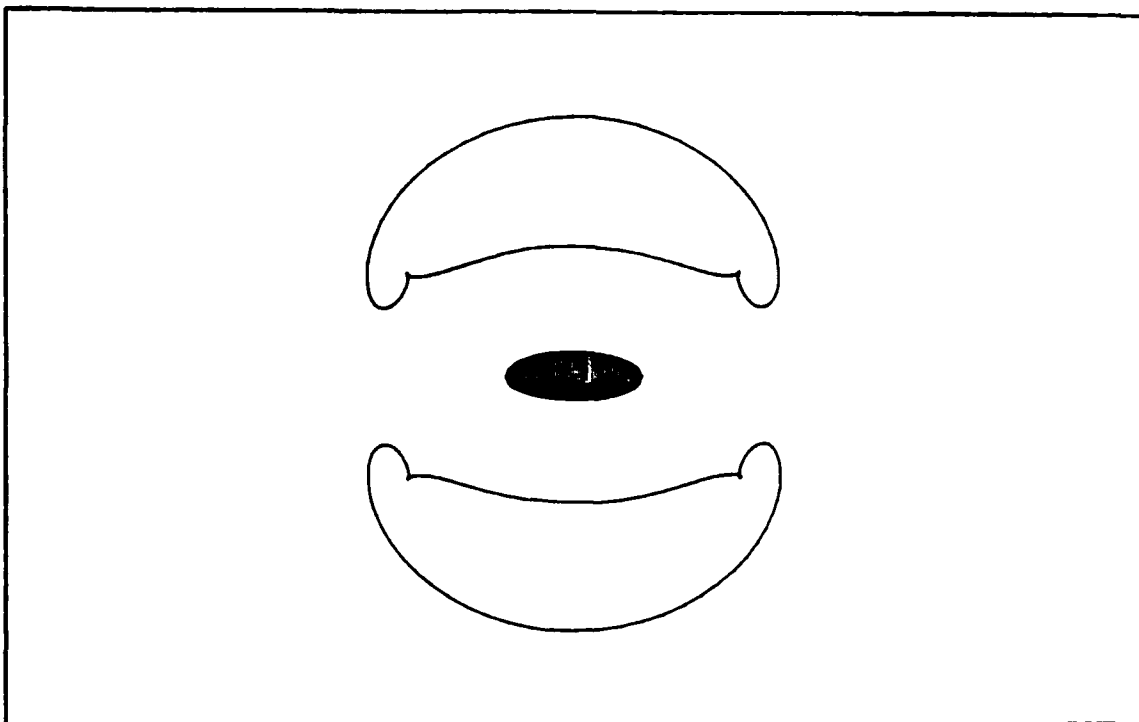


Figure 14: $f = .290 \text{ Rad/TU}$, $R = 1.354845715264 \text{ LU}$,
 $P_{\lambda} = 1.117080805423 \text{ LU}^2/\text{TU}$

Table VI: Summary of Minor Orbits Computed

f (Rad/TU)	R (LU)	P_{λ} (LU ² /TU)	Stability
0.490	1.039041236844	1.000867256234	stable
0.480	1.062624482299	1.012978217714	stable
0.470	1.067382477069	1.019509104377	stable
0.460	1.046834141438	1.019299715560	unstable
0.450	0.986160355569	1.005650561067	unstable
0.449	0.977985586688	1.003324500188	unstable
0.441	0.900412010677	0.977219955036	unstable
0.440	0.888168589907	0.972473210712	unstable
0.440	1.238387157667	1.056690380877	stable
0.435	1.082095823329	0.991288299428	stable
0.435	1.227741787424	1.059177135627	stable
0.430	1.222281650472	1.061495283471	stable
0.425	1.219455010081	1.063773482440	stable
0.420	1.218033152644	1.066023461238	stable
0.415	1.217344653087	1.068234383201	stable
0.410	1.216985353084	1.070392195973	stable
0.405	1.216688740817	1.072483329113	stable
0.400	1.216261042734	1.074494680583	stable
0.395	1.215545133971	1.076412660583	stable
0.394	1.215354721541	1.076783747396	unstable

(Table continued on next page)

Table VI (Continued):

f (Rad/TU)	R (LU)	P_λ (LU ² /TU)	Stability
0.392	1.214917630362	1.077512354812	unstable
0.390	1.214397843252	1.078221895716	unstable
0.360	1.187912621470	1.085107385175	unstable
0.340	1.117341867891	1.077631737758	unstable
0.330	1.038614678848	1.059840481020	unstable
0.325	0.984840557323	1.044125555788	unstable
0.321	1.019464633106	0.896078589786	unstable
0.320	1.029113207899	0.897003545851	unstable
0.319	1.039006180956	0.897988374479	unstable
0.315	1.081426148767	0.902665051849	unstable
0.310	1.130850261552	0.909059307428	unstable
0.307	1.195416827916	0.918602755456	unstable
0.305	1.239528500246	0.925533794275	unstable
0.302	1.350055576137	0.942682054990	unstable
0.300	1.390296759434	1.113911631307	stable
0.290	1.354845715264	1.117080805423	stable
0.280	1.326851733481	1.118784303008	unstable
0.270	1.296053037078	1.119238555695	unstable

V. Major Orbits

Major orbits are those orbits that completely encircle the body. This chapter will present major orbits that lie in the equatorial plane for the example asteroid.

Unlike with the minor orbits, there is not just one \bar{G} vector for the major orbits. The reason for this becomes clear when it is noted that the period of these orbits is actually the synodic period as defined as

$$P_{\text{syn}} = \frac{2\pi}{|\Omega - f|} \quad (5-1)$$

where Ω is the rotational frequency of the asteroid and f is the frequency of the orbit. When $f > \Omega$, the satellite "outruns" the asteroid, implying that the mean radius the orbit is inside the radius for synchronous orbit. Similarly, $f < \Omega$ implies that the mean radius lies outside the synchronous radius.

Thus, referring back to Figure 3 the \bar{G} vector for each case can be easily assembled. If the integration is to be started at $\lambda = \pi/2$, then these vectors are:

$$\bar{G} = \begin{bmatrix} \lambda(t_2) - (3\pi/2) \\ P_{\phi}(t_2) \\ P_R(t_2) \end{bmatrix} \quad \text{for } f > \Omega \quad (5-2a)$$

$$\bar{G} = \begin{bmatrix} \lambda(t_2) + (\pi/2) \\ P_\phi(t_2) \\ P_R(t_2) \end{bmatrix} \quad \text{for } f < \Omega \quad (5-2b)$$

Using these \bar{G} vectors and the method of solution derived in Chapter II, a wide range of major orbits were found. Due to numerical instability, solutions could not be found in the range $.6 < f < 1.45$ rad/TU. However, outside this range, orbits were computed and are presented in the following sections.

Major Orbits With $f > \Omega$

The orbits with a frequency greater than Ω exhibited several interesting characteristics. The first is that they were all stable orbits. The second characteristic is the fact that the paths change shapes considerably over the range of frequencies. Because of this second characteristic, these orbits are grouped by frequency for presentation.

5.2 $> f > 1.97$ Rad/TU. An orbit with a frequency of approximately 5.2 rad/TU just clears the asteroid, so this is upper limit on the frequencies investigated. This orbit is shown in Figure 15. Figures 16 - 18 show the development of the family of orbits as the frequency decreases (and the radius increases). At a frequency of about 2.1 rad/TU, the orbits begin to rapidly change in appearance. Figures 19 - 23 show this trend. Note that in going from a

frequency of 5.2 rad/TU to 1.97 rad/TU, the orbits went from being elongated along the x-axis to being elongated along the y-axis.

1.97 > f > 1.70 Rad/TU. No physically realistic orbits could be found in this range. All orbits found had a shape similar to that of $f = 1.97$ rad/TU, with a radius at $\lambda = \pi$ so small as to cut into the body.

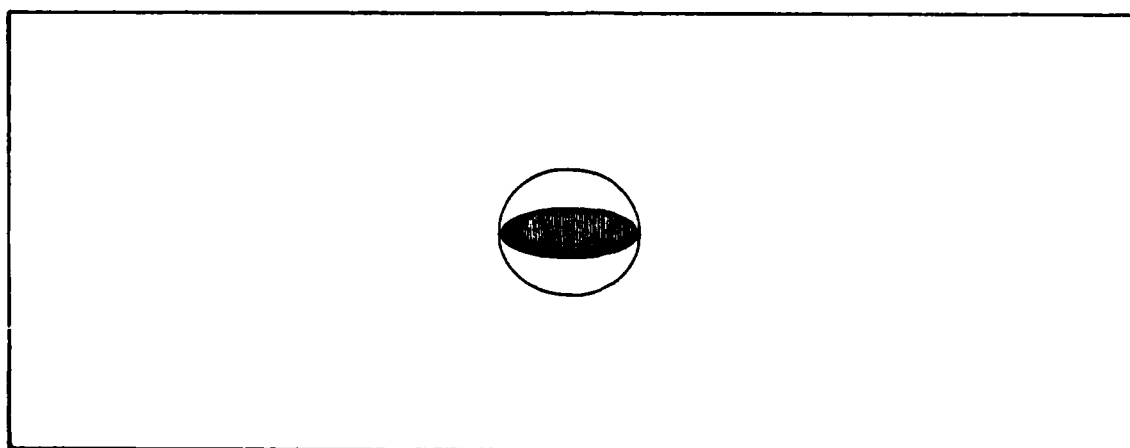


Figure 15: $f = 5.2$ Rad/TU, $R = 0.3285791620856$ LU,
 $P_{\lambda} = 0.5223527976000$ LU²/TU

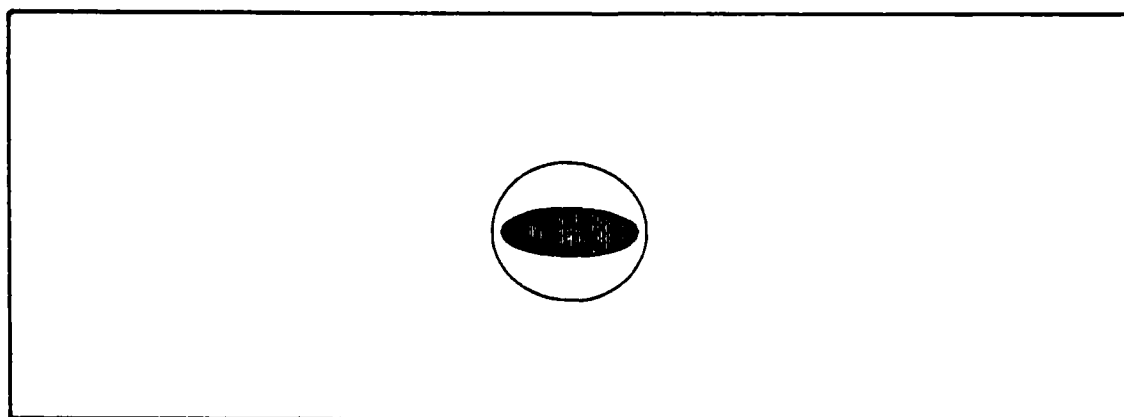


Figure 16: $f = 4.5$ Rad/TU, $R = 0.3660469358352$ LU,
 $P_{\lambda} = 0.5586415882509$ LU²/TU

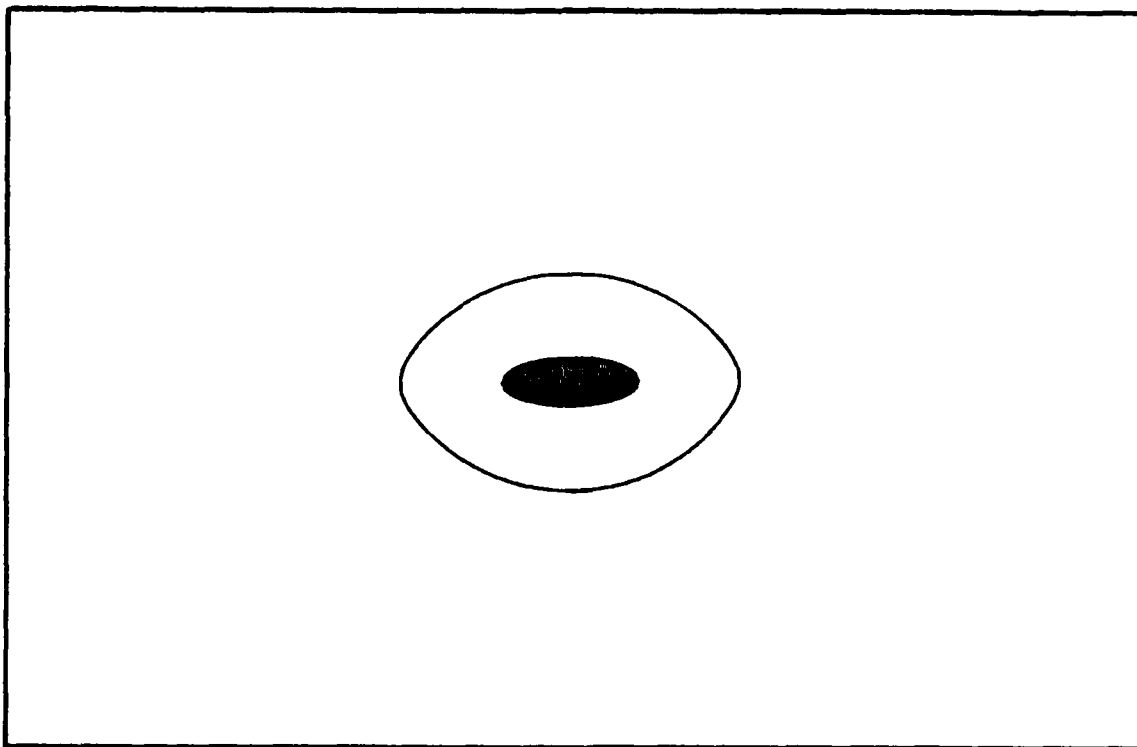


Figure 17: $f = 3.5 \text{ Rad/TU}$, $R = 0.4368881991385 \text{ LU}$,
 $P_{\lambda} = 0.6178884298666 \text{ LU}^2/\text{TU}$

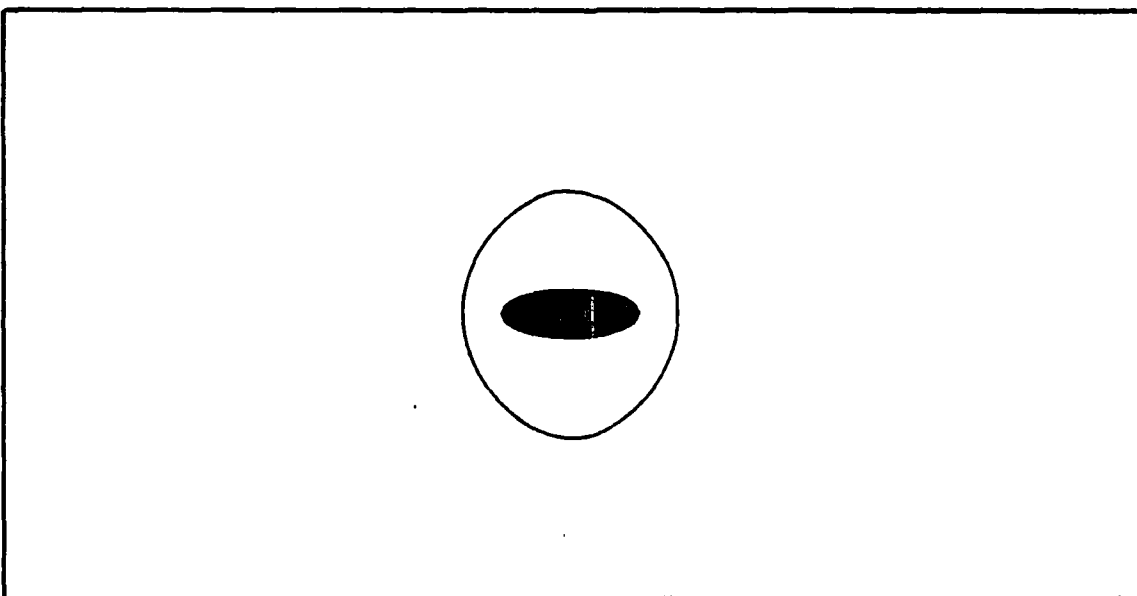


Figure 18: $f = 2.2 \text{ Rad/TU}$, $R = 0.6577526393746 \text{ LU}$,
 $P_{\lambda} = 0.7272907495521 \text{ LU}^2/\text{TU}$

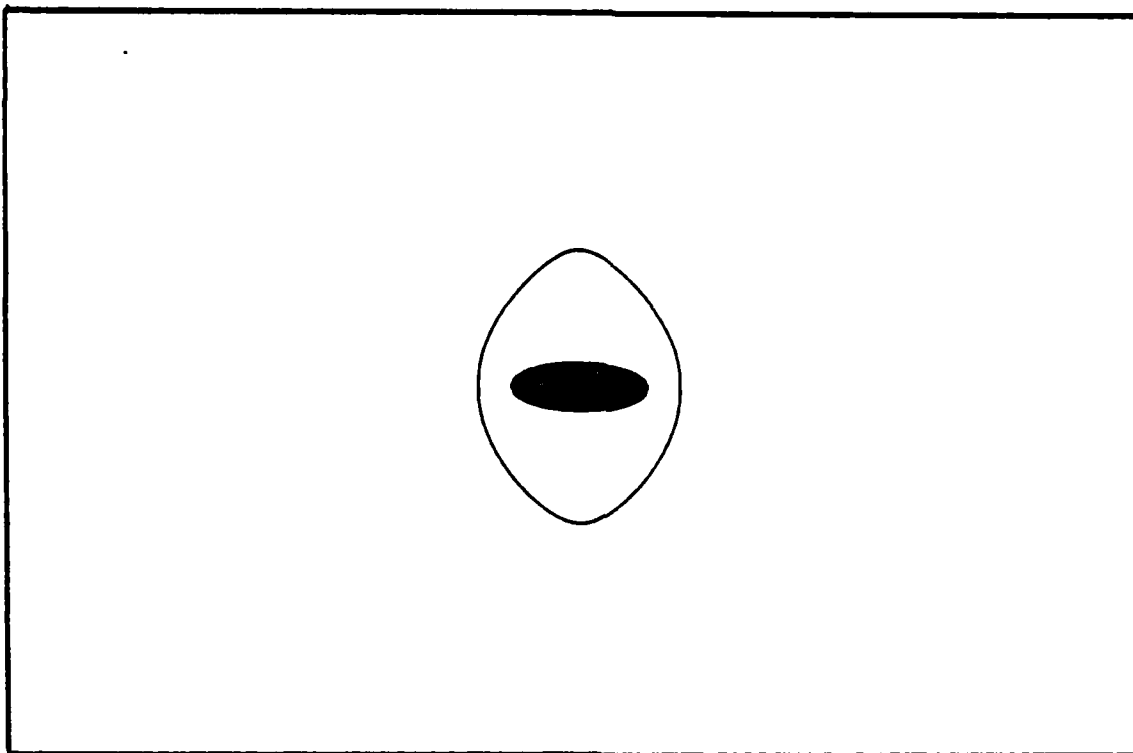


Figure 19: $f = 2.1 \text{ Rad/TU}$, $R = 0.7244296006906 \text{ LU}$,
 $P_{\lambda} = 0.7315590587046 \text{ LU}^2/\text{TU}$

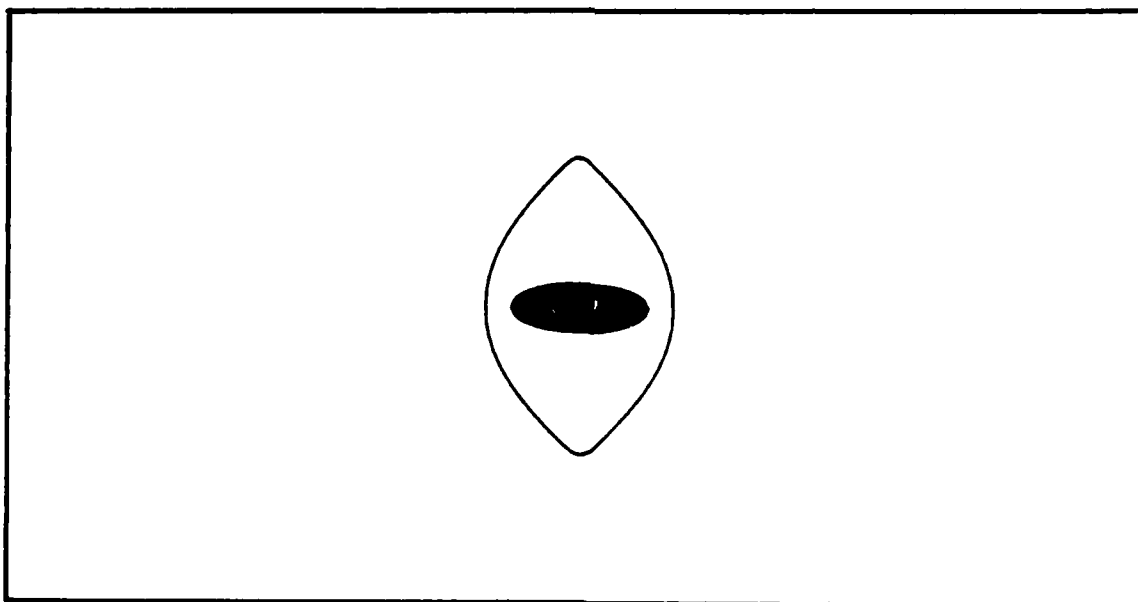


Figure 20: $f = 2.05 \text{ Rad/TU}$, $R = 0.7816397303163 \text{ LU}$,
 $P_{\lambda} = 0.7267807751077 \text{ LU}^2/\text{TU}$

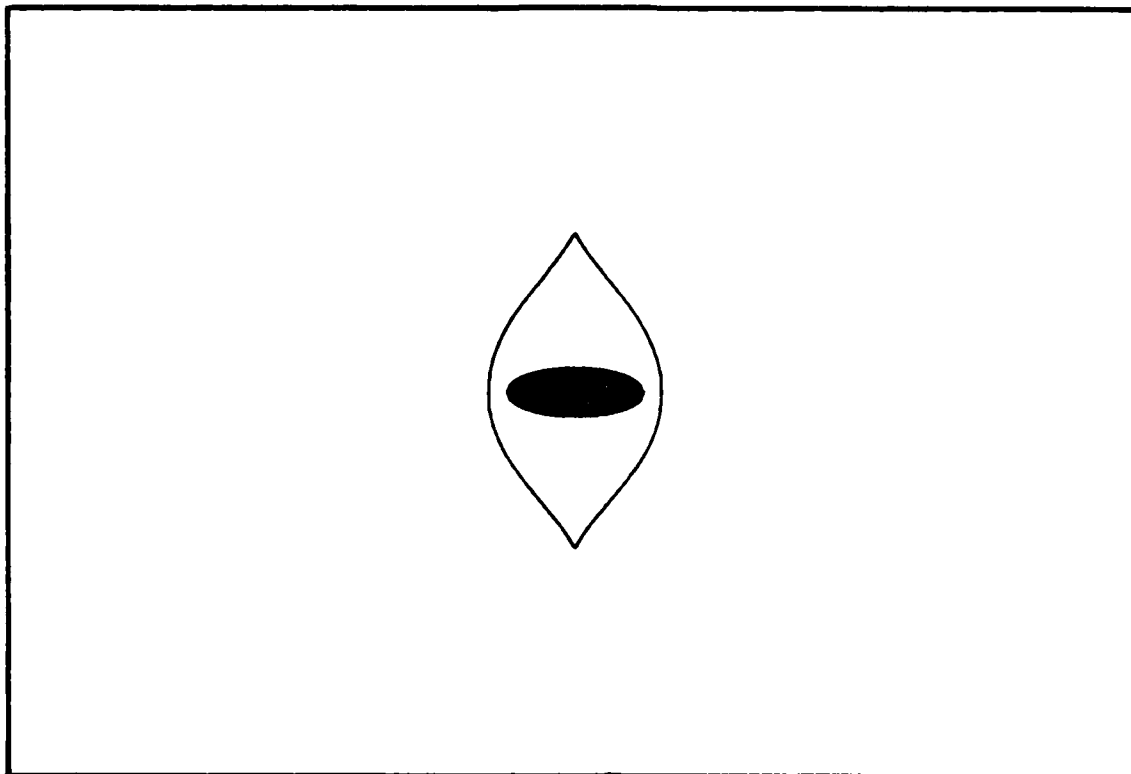


Figure 21: $f = 2.02 \text{ Rad/TU}$, $R = 0.8294374811680 \text{ LU}$,
 $P_{\lambda} = 0.7182213754289 \text{ LU}^2/\text{TU}$

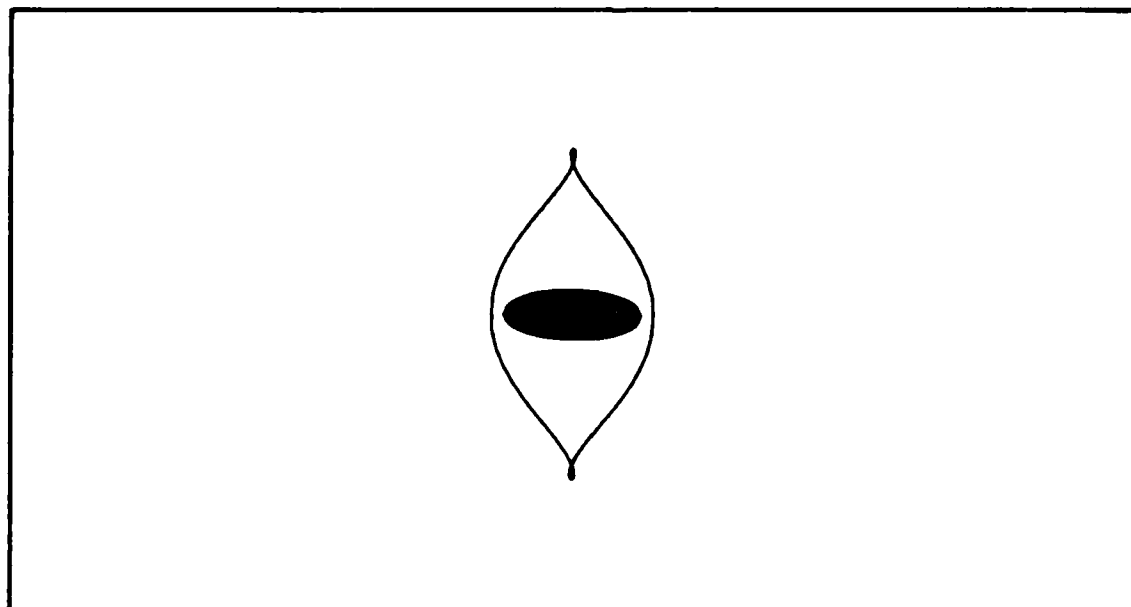


Figure 22: $f = 2.00 \text{ Rad/TU}$, $R = 0.8676722280846 \text{ LU}$,
 $P_{\lambda} = 0.7089389646567 \text{ LU}^2/\text{TU}$

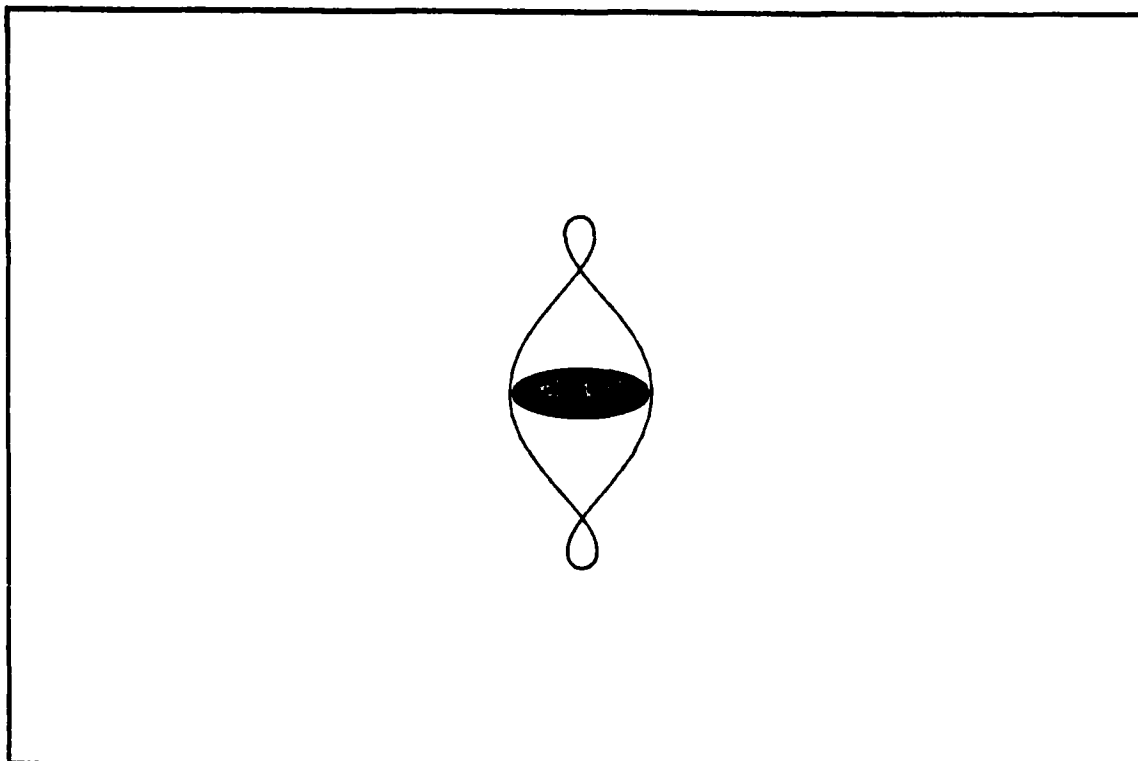


Figure 23: $f = 1.97 \text{ Rad/TU}$, $R = 0.9325366690062 \text{ LU}$,
 $P_\lambda = 0.6892195230246 \text{ LU}^2/\text{TU}$

$1.70 > f > 1.45 \text{ Rad/TU}$. In this range, the orbits take on a simple elliptical shape, as shown in Figures 24 and 25. It is interesting to note that these orbits are, once again, elongated along the x-axis.

$1.45 > f > \Omega \text{ Rad/TU}$. Due to these orbits passing close to the stable equilibrium points, the numerical method used became unstable. Instead of converging on a solution, the iteration scheme diverged. This was most likely due to a singularity in the state transition matrix caused by two or more very close solutions. As a result, no orbits in this range were found.

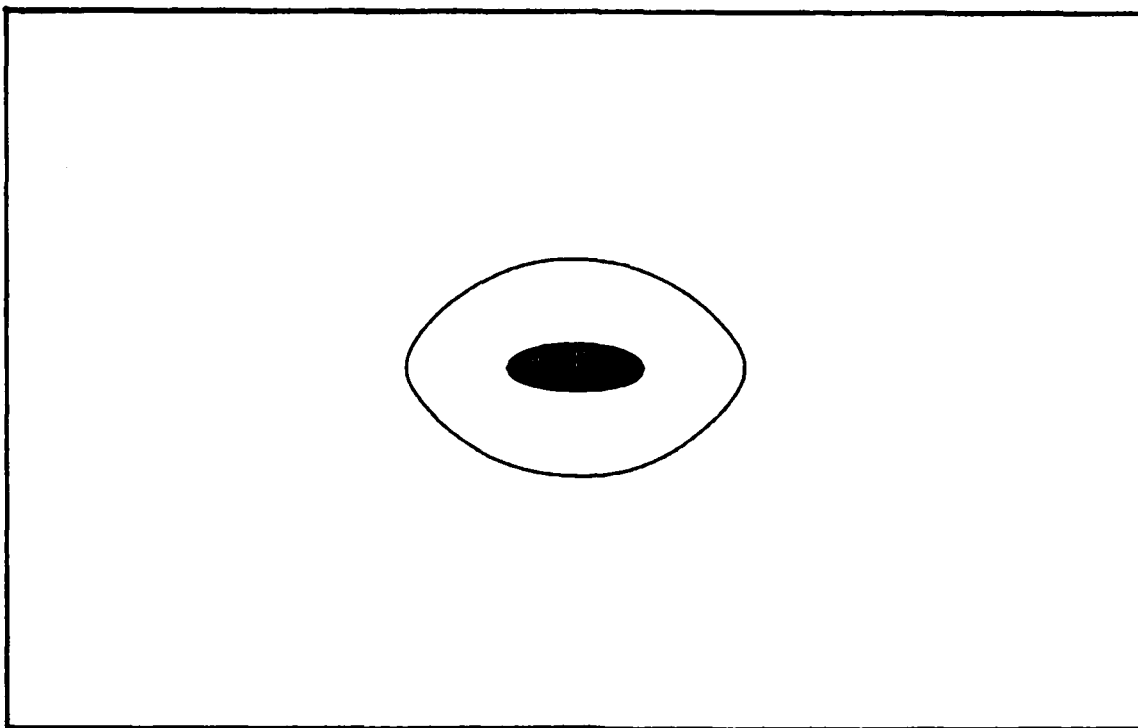


Figure 24: $f = 1.70 \text{ Rad/TU}$, $R = 0.5775263323319 \text{ LU}$,
 $P_{\lambda} = 0.7793806659997 \text{ LU}^2/\text{TU}$

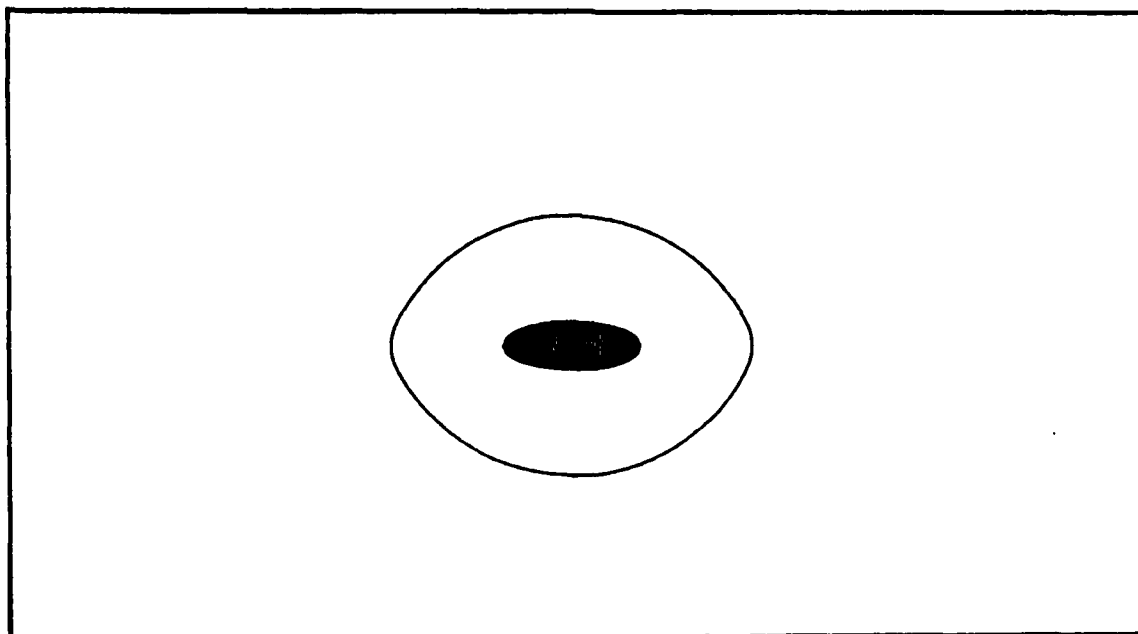


Figure 25: $f = 1.45 \text{ Rad/TU}$, $R = 0.6914873259638 \text{ LU}$,
 $P_{\lambda} = 0.8237375426793 \text{ LU}^2/\text{TU}$

Major Orbits With $f < \Omega$

Unlike the inner orbits, these have almost no variation in shape with frequency. All but one orbit ($f = .5$ rad/sec) computed was stable.

$\Omega > f > 0.6$ Rad/TU. Once again, attempted computation of orbits close to the synchronous radius caused the numerical method to become unstable and diverge. Thus, no closed paths in this range were found.

$0.6 > f$ Rad/TU. As the frequency decreases (and the radius increases), these paths quickly lose their elongation and become almost perfectly circular. This is shown in Figures 26 and 27. It is interesting to note that the only unstable major orbit found occurred at $f = 0.5$ rad/TU.

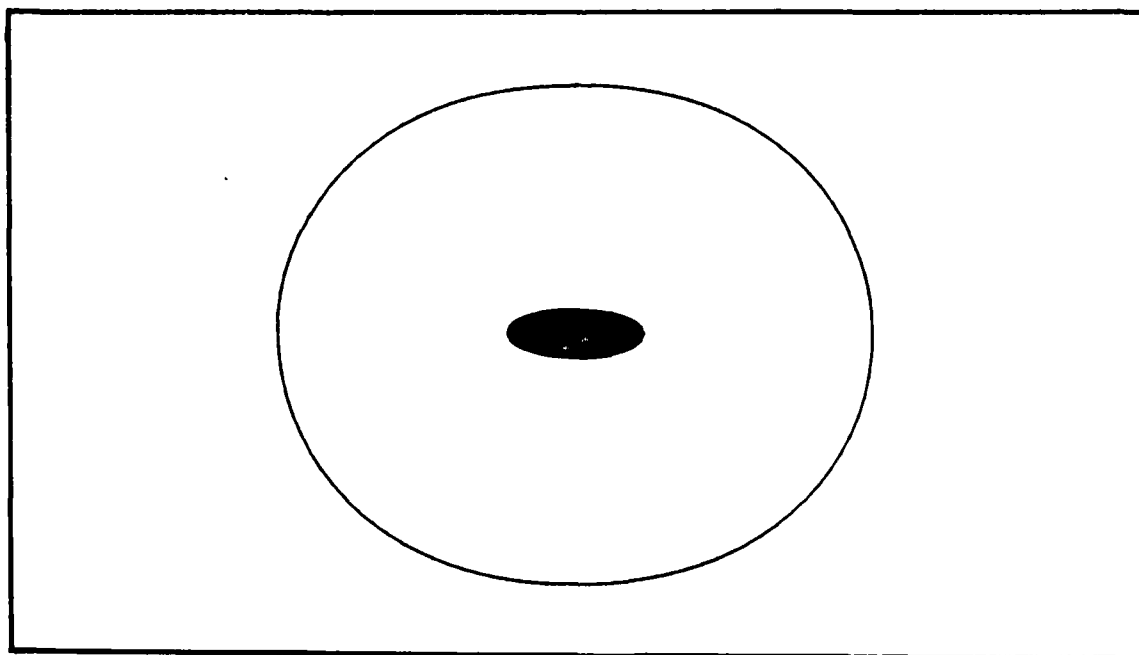


Figure 26: $f = 0.6$ Rad/TU, $R = 1.328869494267$ LU,
 $P_\lambda = 1.198300228534$ LU²/TU

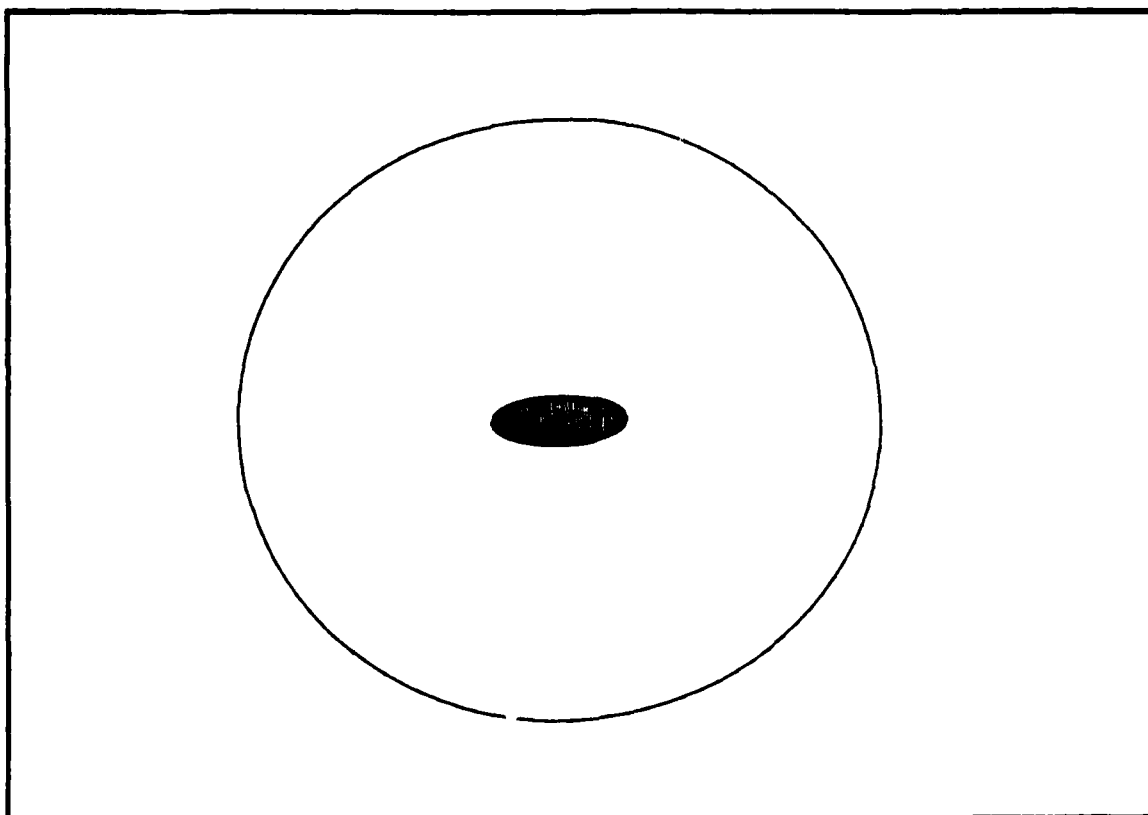


Figure 27: $f = 0.5 \text{ Rad/TU}$, $R = 1.574940235844 \text{ LU}$,
 $P_{\lambda} = 1.271992801430 \text{ LU}^2/\text{TU}$

Remarks on Major Orbits

Figures 28 and 29 graphically summarize all of the major orbits computed in this study. These computations reveal several interesting features of the major orbits. These are:

1. No physically realistic major with frequencies in the range $1.97 > f > 1.70 \text{ rad/TU}$ were found.
2. Interesting phenomena occur near frequencies of 2.0Ω , Ω , and $0.5\Omega \text{ rad/TU}$. At frequencies very

close to $f = 2.0 \Omega \text{ rad/TU}$, the orbits begin to rapidly change their shape. (See Figures 22 - 25.) Near $f = \Omega \text{ rad/TU}$, the method of solution became unstable and diverged. The only unstable major orbit found was at a frequency very close to $f = 0.5 \Omega \text{ rad/TU}$.

3. At frequencies lower than $f = .4 \text{ rad/TU}$, the orbits are essentially circular. Below this, the satellite behaves as if the asteroid were a spherical body.

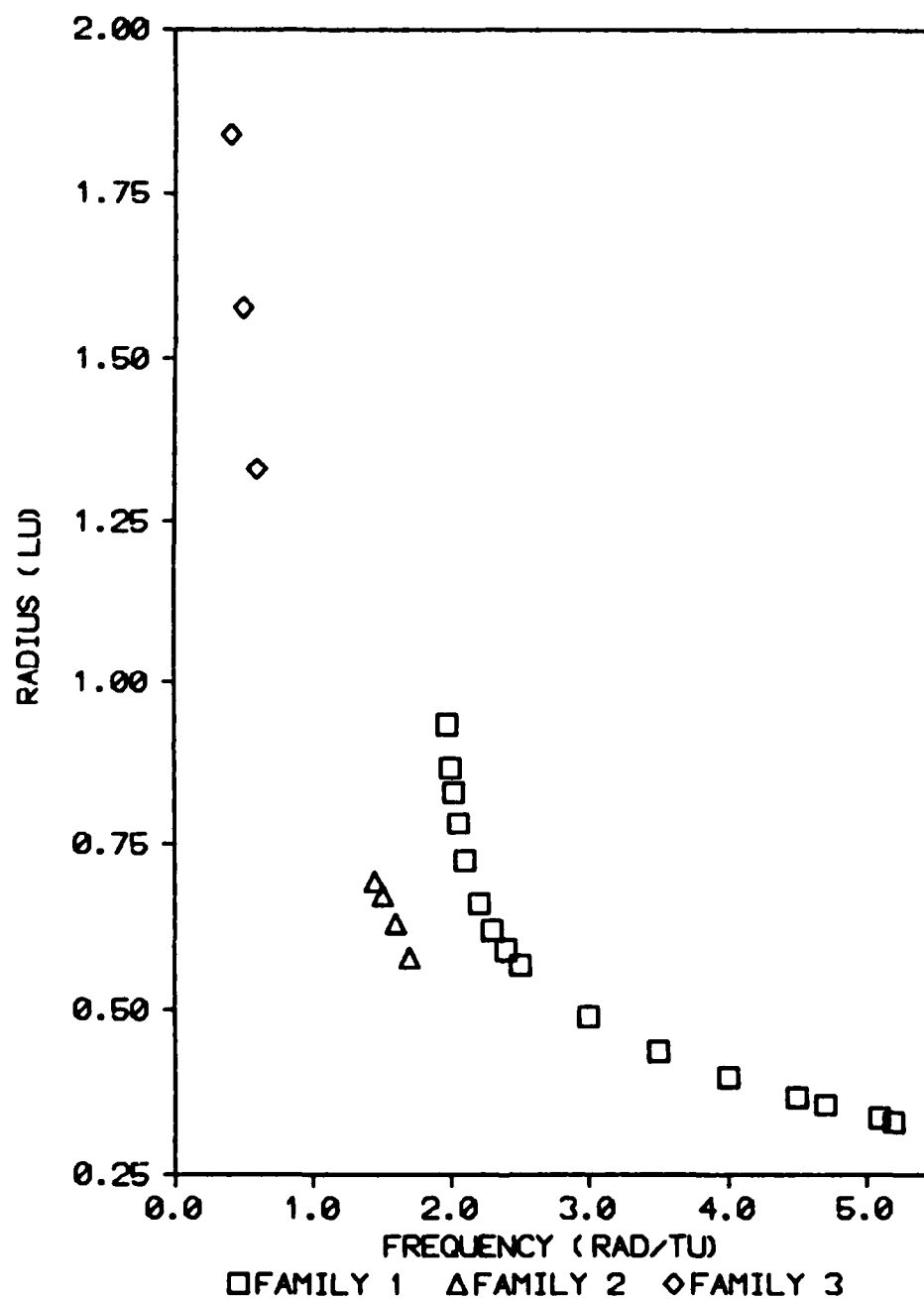


Figure 28: Initial Radius -vs- Frequency

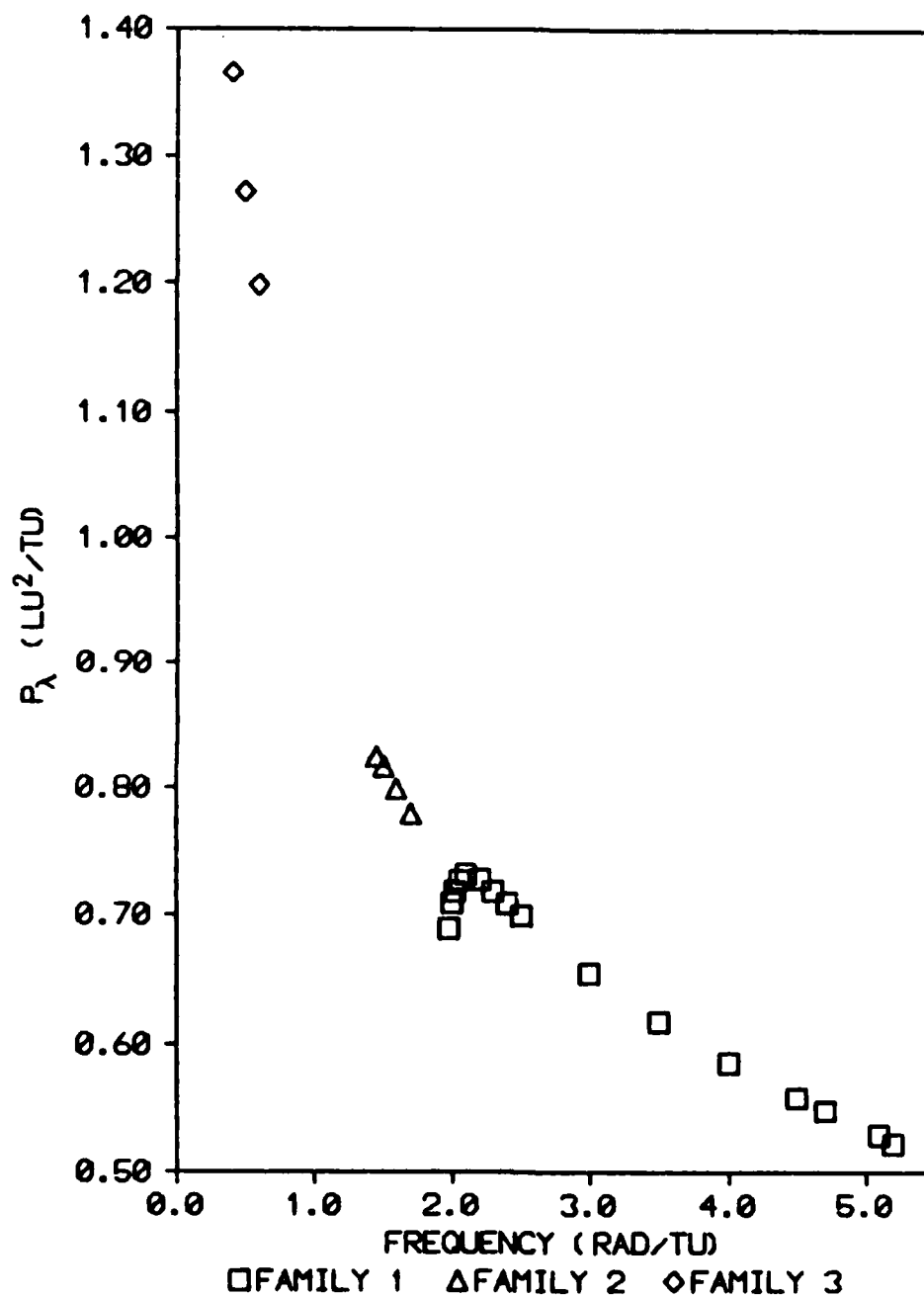


Figure 29: Initial P_λ -vs- Frequency

Conclusion and Recommendations

The key results of this study have been stated in each chapter already, so they will not be repeated in detail here. To summarize the results, each step of the problem solution will be looked at from the aspect of possible future research.

Dynamics and Method of Solution

The equations of motions were derived using a truncated power series expansion for the gravity potential. A future study could retain more terms in the series, but this is not recommended. The inaccuracy introduced by ignoring surface features (craters, etc.) and assuming a triaxial shape for the asteroid is probably greater than that due to the truncated terms.

If major orbits near the synchronous radius are to be investigated in future studies, another method of solution needs to be found. Instead of setting a period and iterating on ϕ , R , and P_λ , it might be advantageous to set R and iterate on ϕ , P_λ , and the period.

Equilibrium Points

The equilibrium points were fully investigated. No further study is recommended.

Minor Orbits

The study of the minor orbits produced a host of seemingly unrelated paths. These orbits should be investigated in more depth to see if any relationships can be found. Additionally, inclined orbits should be investigated.

Major Orbits

If a new method of solution that remains stable near the synchronous radius is developed, then the major orbits in this region should be investigated. Once again, inclined orbits should also be investigated.

Related Problem for Study

An interesting extension of this research would be to include the gravitational effects of a nearby planet. Thus, orbits about such bodies as Phobos and Deimos (Martian moons) could be investigated.

Conclusion

This study found the governing equations for the motion of a small satellite about a rotating asteroid. Methods were then employed to solve these in such a way as to find the equilibrium points, minor orbits about the stable equilibrium points, and major orbits for a fictitious asteroid. All orbits found were in the equatorial plane of the asteroid.

Appendix A: Fictitious Asteroid Characteristics

Any real asteroid could have been selected to use as an example, but Hektor was originally selected due to the fact that it is one of the more ellipsoidal bodies. It was found, however, that by using a slower rotation rate, the dynamics produced more extreme behavior. For this reason, a fictitious asteroid was invented with the dimensions of Hektor and a slower rotation rate. The physical characteristics of this body are given in Table VII.

Table VII: Fictitious Asteroid Data (Standard Units)

a (km)	b (km)	c (km)	Ω (rad/s)	Mass (kg)
170.0	63.9	56.5	$2\pi \times 10^{-5}$	7.33×10^{18}

For numerical reasons, it is desirable to convert to a canonical system of units that allows the integration to be performed with numbers of approximately the same order of magnitude. Appropriate length units (LUs), time units (TUs), and mass units (MUs) can easily be found to accomplish this. If one length unit is defined as the radius of a synchronous circular orbit about an equivalent spherical body and if it is desired to set $Gm_2 = 1 \text{ LU}^3/\text{TU}^2$, then the

following conversion factors for length, time, and mass units can be found:

$$\begin{aligned}1 \text{ LU} &= 467.8 \text{ km} \\1 \text{ TU} &= 1.592 \times 10^4 \text{ sec} \\1 \text{ MU} &= 7.33 \times 10^{18} \text{ kg}\end{aligned}\tag{A-1}$$

After converting the the values in Table VII to these units, the moments of inertia can also be calculated. The physical data in these new units are given in Table VIII. These values were considered to be exact and were used in all of the example calculations.

Table VIII: Fictitious Asteroid Data (Canonical Units)

$$\begin{aligned}a &= 0.341 \text{ LU} \\b &= 0.128 \text{ LU} \\c &= 0.113 \text{ LU} \\I_{xx} &= 5.86 \times 10^{-3} \text{ LU}^2 \cdot \text{MU} \\I_{yy} &= 2.58 \times 10^{-2} \text{ LU}^2 \cdot \text{MU} \\I_{zz} &= 2.65 \times 10^{-2} \text{ LU}^2 \cdot \text{MU} \\\Omega &= .3184\pi \text{ rad/TU} \\G &= 1 \text{ MU} \cdot \text{LU}^3 / \text{TU}^2\end{aligned}$$

Appendix B: Variational Matrix

Terms of A Matrix:

$$a_{11} = 0 \qquad a_{12} = \frac{2P_{\lambda} \sin \phi}{R^2 \cos^3 \phi} \qquad a_{13} = \frac{-2P_{\lambda}}{R^3 \cos^2 \phi}$$

$$a_{14} = \frac{1}{R^2 \cos^2 \phi} \qquad a_{15} = 0 \qquad a_{16} = 0$$

$$a_{21} = 0 \qquad a_{22} = 0 \qquad a_{23} = \frac{-2P_{\phi}}{R^3}$$

$$a_{24} = 0 \qquad a_{25} = \frac{1}{R^2} \qquad a_{26} = 0$$

$$a_{31} = 0 \qquad a_{32} = 0 \qquad a_{33} = 0$$

$$a_{34} = 0 \qquad a_{35} = 0 \qquad a_{36} = 1$$

$$a_{41} = \frac{3G}{R^3} (I_{xx} - I_{yy}) (\cos^2 \lambda - \sin^2 \lambda) \cos^2 \phi$$

$$a_{42} = \frac{6G}{R^3} (I_{yy} - I_{xx}) \cos \phi \sin \phi \cos \lambda \sin \lambda$$

$$a_{43} = \frac{9G}{R^4} (I_{yy} - I_{xx}) \cos^2 \phi \cos \lambda \sin \lambda$$

$$a_{44} = 0$$

$$a_{45} = 0$$

$$a_{46} = 0$$

$$a_{51} = \frac{6G}{R^3} (I_{yy} - I_{xx}) \cos \phi \sin \phi \cos \lambda \sin \lambda$$

$$a_{52} = \frac{-P_{\lambda}^2}{R^2 \cos^2 \phi} - \frac{3P_{\lambda}^2 \sin^2 \phi}{R^2 \cos^4 \phi} - \frac{3G}{2R^3} [(\cos^2 \lambda - \sin^2 \lambda) (I_{yy} - I_{xx}) \\ + (2I_{zz} - I_{xx} - I_{yy})] (\cos^2 \phi - \sin^2 \phi)$$

$$a_{53} = \frac{2P_{\lambda}^2 \sin \phi}{R^3 \cos^3 \phi} + \frac{9G}{2R^4} [(\cos^2 \lambda - \sin^2 \lambda) (I_{yy} - I_{xx}) \\ + (2I_{zz} - I_{xx} - I_{yy})] \cos \phi \sin \phi$$

$$a_{54} = - \frac{2P_{\lambda} \sin \phi}{R^2 \cos^3 \phi}$$

$$a_{55} = 0$$

$$a_{56} = 0$$

$$a_{61} = \frac{9G}{R^4} (I_{YY} - I_{XX}) \cos\lambda \sin\lambda \cos^2\phi$$

$$a_{62} = \frac{2P_{\lambda}^2 \sin\phi}{R^3 \cos^3\phi} - \frac{9G}{2R^4} [(I_{YY} - I_{XX}) (\sin^2\lambda - \cos^2\lambda) \\ + (I_{XX} + I_{YY} - 2I_{ZZ})] \cos\phi \sin\phi$$

$$a_{63} = \frac{2Gm_2}{R^3} + \frac{3G}{R^5} [(3\cos^2\phi \cos^2\lambda - 1) (I_{YY} + I_{ZZ} - I_{XX}) \\ + (3\cos^2\phi \sin^2\lambda - 1) (I_{XX} + I_{ZZ} - I_{YY}) \\ + (3\sin^2\phi - 1) (I_{XX} + I_{YY} - I_{ZZ})] \\ - \frac{3P_{\lambda}^2}{R^4 \cos^2\phi} - \frac{3P_{\phi}^2}{R^4}$$

$$a_{64} = \frac{2P_{\lambda}}{R^3 \cos^2\phi}$$

$$a_{65} = \frac{2P_{\phi}}{R^3}$$

$$a_{66} = 0$$

Bibliography

1. Chapman, C. R. "Asteroid," McGraw-Hill Encyclopedia of Astronomy. New York: McGraw-Hill Book Company, 1983.
2. Dobrovolskis, A. R. "Internal Stresses in Phobos and Other Triaxial Bodies," Icarus, Volume 52: 136-148 (October 1982).
3. Kammeyer, P. C. "Periodic Orbits Around a Rotating Ellipsoid," Celestial Mechanics, Volume 17: 37-48 (January 1978).
4. Meirovitch, Leonard. Methods of Analytical Dynamics. New York: McGraw-Hill Book Company, 1970.
5. Wiesel, W. Lecture material covered in MC636, Advanced Astrodynamics. School of Engineering, Air Force Institute of Technology (AU), Wright-Patterson AFB OH, January 1986.
6. Wiesel, W. Lecture material distributed in MC636, Advanced Astrodynamics. School of Engineering, Air Force Institute of Technology (AU), Wright-Patterson AFB OH, January 1986.
7. Zappala, V. and Knezevic, Z. "Rotation Axes of Asteroids: Results for 14 Objects," Icarus, Volume 59: 436-453 (September 1984).
8. Zhuravlev, S. G. "About the Stability of the Libration Points of a Rotating Triaxial Ellipsoid in a Degenerate Case," Celestial Mechanics, Volume 8: 75-84 (August 1973).
9. Zhuravlev S. G. and Zlenko, A. A. "Conditionally Periodic, Translational-rotational Motions of a Satellite of a Triaxial Planet," Soviet Astronomy, Volume 27: 707-710 (November-December 1983).

Vita

Lieutenant Kerry D. Hicks was born 6 October 1962 in Cordell, Oklahoma. He graduated from high school in O'Fallon, Illinois in 1981. The same year, he was admitted to the University of Illinois in Urbana-Champaign, Illinois. From there, he received a Bachelor of Science in Aeronautical and Astronautical Engineering with honors and was commissioned in the USAF through the ROTC program in May of 1985. Lt Hicks also entered the School of Engineering, Air Force Institute of Technology in May of 1985.

Permanent Address: 1512 Princeton Dr
O'Fallon, IL 62269

REPORT DOCUMENTATION PAGE

Form Approved
OMB No. 0704-0188

1a. REPORT SECURITY CLASSIFICATION UNCLASSIFIED			1b. RESTRICTIVE MARKINGS		
2a. SECURITY CLASSIFICATION AUTHORITY			3. DISTRIBUTION / AVAILABILITY OF REPORT Approved for public release; distribution unlimited.		
2b. DECLASSIFICATION / DOWNGRADING SCHEDULE					
4. PERFORMING ORGANIZATION REPORT NUMBER(S) AFIT/GA/AA/86D-7			5. MONITORING ORGANIZATION REPORT NUMBER(S)		
6a. NAME OF PERFORMING ORGANIZATION School of Engineering		6b. OFFICE SYMBOL (If applicable) AFIT/ENY		7a. NAME OF MONITORING ORGANIZATION	
6c. ADDRESS (City, State, and ZIP Code) Air Force Institute of Technology Wright-Patterson AFB, Ohio 45433				7b. ADDRESS (City, State, and ZIP Code)	
8a. NAME OF FUNDING / SPONSORING ORGANIZATION		8b. OFFICE SYMBOL (If applicable)		9. PROCUREMENT INSTRUMENT IDENTIFICATION NUMBER	
8c. ADDRESS (City, State, and ZIP Code)				10. SOURCE OF FUNDING NUMBERS	
				PROGRAM ELEMENT NO.	PROJECT NO.
11. TITLE (Include Security Classification) See Box 19					
12. PERSONAL AUTHOR(S) Hicks, Kerry Douglas, B.S., 2Lt, USAF					
13a. TYPE OF REPORT MS Thesis		13b. TIME COVERED FROM _____ TO _____		14. DATE OF REPORT (Year, Month, Day) 1986 December	
15. PAGE COUNT 74					
16. SUPPLEMENTARY NOTATION <i>(cont'd fr p 65)</i>					
17. COSATI CODES			18. SUBJECT TERMS (Continue on reverse if necessary and identify by block number)		
FIELD	GROUP	SUB-GROUP	Asteroids, Equilibrium Points; Periodic Orbits; Triaxial Ellipsoids. (THREE) A		
22	01				
22	03				
19. ABSTRACT (Continue on reverse if necessary and identify by block number)					
Title: PERIODIC ORBITS ABOUT ROTATING ASTEROIDS IN FREE SPACE					
Thesis Advisor: William Wiesel Associate Professor of Astronautics					
Approved for public release: LAW AFR 190-1/ L. E. WOLAVER 13 MAR 87 Dean for Research and Professional Development Air Force Institute of Technology (AFIT) Wright-Patterson AFB OH 45433					
20. DISTRIBUTION / AVAILABILITY OF ABSTRACT <input checked="" type="checkbox"/> UNCLASSIFIED/UNLIMITED <input type="checkbox"/> SAME AS RPT. <input type="checkbox"/> DTIC USERS			21. ABSTRACT SECURITY CLASSIFICATION UNCLASSIFIED		
22a. NAME OF RESPONSIBLE INDIVIDUAL William Wiesel, Associate Professor			22b. TELEPHONE (Include Area Code) (513) 255-3517		22c. OFFICE SYMBOL AFIT/ENY

Block 19:

✓
In This investigation of

This study investigated periodic orbits about asteroids rotating in free space, oscillatory orbits about equilibrium points as well as those orbits encircling the body were found. While a method was derived for finding orbits of all inclinations, only equatorial orbits are presented, in this report. The major emphasis is on stable, periodic orbits, but certain unstable orbits are presented where appropriate.

The analysis assumed that asteroids could be represented by triaxial ellipsoidal bodies rotating about their major axis of inertia. Hamilton's canonical equations were derived to describe the dynamics. An algorithm was then developed and used to solve the equations of motion in such a way as to find closed, periodic orbits.

Keywords:

(1) (2) (3) (4) (5) (6) (7) (8) (9) (10) (11) (12) (13) (14) (15) (16) (17) (18) (19) (20) (21) (22) (23) (24) (25) (26) (27) (28) (29) (30) (31) (32) (33) (34) (35) (36) (37) (38) (39) (40) (41) (42) (43) (44) (45) (46) (47) (48) (49) (50) (51) (52) (53) (54) (55) (56) (57) (58) (59) (60) (61) (62) (63) (64) (65) (66) (67) (68) (69) (70) (71) (72) (73) (74) (75) (76) (77) (78) (79) (80) (81) (82) (83) (84) (85) (86) (87) (88) (89) (90) (91) (92) (93) (94) (95) (96) (97) (98) (99) (100)

END

5-87

DTIC